J. Membrane Biol. 92, 91–110 (1986)

The Journal of
Membrane Biology

Interpretation of Steady-State Current-Voltage Curves: Consequences and Implications of Current Subtraction in Transport Studies

Michael R. Blatt
Botany School, University of Cambridge, Cambridge CB2 3EA, United Kingdom

Summary. A problem often confronted in analyses of charge-carrying transport processes *in vivo* lies in identifying porter-specific component currents and their dependence on membrane potential. Frequently, current-voltage (*I-V*)—or more precisely, difference-current-voltage (*dI-V*)—relations, both for primary and for secondary transport processes, have been extracted from the overall membrane current-voltage profiles by subtracting currents measured before and after experimental manipulations expected to alter the porter characteristics only. This paper examines the consequences of current subtraction within the context of a generalized kinetic carrier model for Class I transport mechanisms (U.-P. Hansen, D. Gradmann, D. Sanders and C.L. Slayman, 1981, *J. Membrane Biol.* **63**:165–190). Attention is focused primarily on *dI-V* profiles associated with ion-driven secondary transport for which external solute concentrations usually serve as the experimental variable, but precisely analogous results and the same conclusions are indicated in relation to studies of primary electrogenesis. The model comprises a single transport loop linking *n* (3 or more) discrete states of a carrier 'molecule.' State transitions include one membrane charge-transport step and one solute-binding step. Fundamental properties of *dI-V* relations are derived analytically for all *n*-state formulations by analogy to common experimental designs. Additional features are revealed through analysis of a "reduced" 2-state empirical form, and numerical examples, computed using this and a "minimum" 4-state formulation, illustrate *dI-V* curves under principle limiting conditions. Class I models generate a wide range of *dI-V* profiles which can accommodate essentially all of the data now extant for primary and secondary transport systems, including difference current relations showing regions of negative slope conductance. The particular features exhibited by the curves depend on the relative magnitudes and orderings of reaction rate constants within the transport loop. Two distinct classes of *dI-V* curves result which reflect the relative rates of membrane charge transit and carrier recycling steps. Also evident in difference current relations are contributions from 'hidden' carrier states not directly associated with charge translocation in circumstances which can give rise to observations of counterflow or exchange diffusion. Conductance-voltage relations provide a semi-quantitative means to obtaining pairs of empirical rate parameters. It is demonstrated that *dI-V* relations *cannot* yield directly meaningful transport reversal potentials in most common experimental situations. Well-defined arrangements of reaction constants are shown to give *dI-V* curves which exhibit little or no voltage sensitivity and finite currents over many tens to hundreds of millivolts *including* the true reversal potential. Furthermore, difference currents show apparent Michaelian kinetics with solute concentration at *all* membrane potentials. These findings bring into question several previous reports of reversal potentials, stoichiometries and apparent current-source behavior based primarily on difference current analysis. They also provide a coherent explanation for anomolous and shallow conductances and paradoxical situations in which charge stoichiometry varies with membrane potential.

Key Words electrogenic transport · reaction kinetic model · conductance-voltage curve · equilibrium potential · equilibrium binding · solute/substrate concentration

Introduction

It is now generally recognized that the vast majority of membrane transport processes in living cells involve the movement of charge. In prokaryotes, redox-driven (proton) transport provides the primary driving force for metabolite uptake (Foster & Fillingame, 1979). In eukaryotes primary electrochemical gradients of Na^+ in animals and H^+ in plants and fungi are generated by the Na^+, K^+- and H^+-ATPases, respectively (Skou & Norby, 1979; Bentrup, 1980; Goffeau & Slayman, 1981). Likewise, coupling solute uptake to the downhill movement of Na^+ or H^+ in "active" transport generally also entails charge flow (Epstein, 1976; Eddy, 1978; West, 1980). This pattern is true for the translocation of neutral metabolites, such as sugars (Komor & Tanner, 1974, 1980; Kinne, 1976; Hansen & Slayman, 1978; Kaczorowski et al., 1980), as well as for charged species, including amino acids (Lanyi, 1978; Felle, 1981*a*; Page & West, 1981; Sanders et al., 1983; Jung et al., 1984; Johannes & Felle, 1985), nucleotide precursors (Reichert et al., 1975), and inorganic ions (Lanyi & MacDonald, 1976; Sanders, 1980*a*,*b*; Milanick & Gunn, 1982; Blatt et al., 1984; Lass & Ullrich-Eberius, 1984; Ullrich-Eberius et al., 1984).

Understanding the contribution of the membrane electric field to solute translocation is thus fundamental and has provided impetus to incorporate the electrical parameter into a general description of vectorial enzyme kinetics. From the kinetic viewpoint, membrane potential (inside negative) enters into each of these processes either as a "product," in the case of primary electrogenesis, or as a "substrate" for secondary transport. Transmembrane charge flux (current), in turn, is the electrical counterpart to transport velocity. Finkelstein (1964) first introduced voltage using a diffusion paradigm, and more recent models have developed around concepts of pores (Läuger, 1979, 1980) and carriers (Läuger & Stark, 1970; Chapman et al., 1979, 1983; Hansen et al., 1981; Chapman, 1982). In general, all of these models are competent to account for the primary feature of charge translocators, that of current saturation observed in the steady state at voltage extremes. Applications of one formulation (Hansen et al., 1981; Sanders et al., 1984), in particular, have yielded simple kinetic interpretations for postulates such as ion wells (Mitchell, 1969; Komor & Tanner, 1980; Maloney, 1982), stoichiometry changes (LeBlanc et al., 1980) and carrier-mediated "leakage" (Eddy, 1980). Furthermore, statistically optimizing experimentally derived current-voltage data have indicated sites for principle rate-limiting steps associated with electrogenic H^+ transport in *Neurospora* and Cl^- transport in *Acetabularia* (Gradmann et al., 1982).

For the majority of steady-state current-voltage (*I-V*) studies carried out to date, however, the fundamental difficulty has been in simply extracting, from the overall *I-V* relations of the biological membranes, the *I-V* characteristics specific to a single transport process. This problem has been most acutely felt in studies of plant cells and microorganisms for which, unlike most animal tissues (*cf.* Marmor, 1971; Kostyuk et al., 1972; Mandel & Curran, 1973; Fuchs et al., 1977; Roy & Okada, 1978; Goudeau et al., 1982; *see also* Chapman et al., 1979), voltage spans of 200 to 300 mV are generally accessible (Gradmann, 1975; Gradmann et al., 1978; Felle, 1981*a*, 1982), and from which a corresponding degree of kinetic information might be gained.

The most common approach to extracting *I-V* relations is current subtraction which yields transport-specific difference-current-voltage (*dI-V*) curves. Conceptually as well as experimentally the approach is straightforward. Whole membrane *I-V* relations are determined by conventional voltage-clamp techniques both in the presence and absence of a porter-specific modifier (e.g., a substrate or inhibitor). The difference between the two curves is then obtained across the available voltage spectrum by subtracting the respective currents at every membrane potential. Difference *I-V* characteristics derived in this fashion have been used to characterize both primary electrogenic ion pumps and secondary transport of organic and inorganic solutes in the fungus *Neurospora* (Gradmann et al., 1978; Hansen & Slayman, 1978; Sanders et al., 1983; Blatt et al., 1984; Blatt & Slayman, 1986), the giant algae *Acetabularia* (Gradmann, 1975) and *Chara* (Walker et al., 1979; Beilby & Walker, 1981; Beilby, 1984; Kishimoto et al., 1984; Takeuchi et al., 1985), and a liverwort, *Riccia* (Felle, 1980, 1981*a*,*b*; Johannes & Felle, 1985). Current subtractions of steady-state *I-V* curves have also been used to extract voltage-dependent features for active Na^+ transport in snail neurones (Kostyuk et al., 1972), a putative K^+ conductance in L-cells (Roy & Okada, 1978), and ionic components of transcellular pathways in frog skin (Fuchs et al., 1977; Goudeau et al., 1982).

Now, there are two main assumptions which underly current subtraction. The first and most obvious prerequisite is that current passage through the porter in question only should change during the course of modifier treatment—specifically over the time frame in which *I-V* scans are performed. Clearly, if secondary conductance changes accompany the treatment, current subtraction will not eliminate their component *I-V* characteristics in the difference curve. Consequently, most studies of this kind have been carried out over short time intervals (Gradmann et al., 1978, 1982; Sanders et al., 1983; Blatt et al., 1984; Blatt & Slayman, 1986), although the point has been stretched to extremes in at least one study of the *Chara* proton pump (Kishimoto et al., 1984; Takeuchi et al., 1985). [An important corollary to this assumption for inhibitor studies is that the drugs used are specific for the porter. This criterion is met in practice with ouabain inhibition of the Na^+, K^+-ATPase in animal tissues (Skou & Norby, 1979; Karlish & Stein, 1982).]

It is the second, and more subtle assumption which will be the focus of this paper. This assumption states that changes in the *I-V* characteristic of the porter in question brought about during experimental manipulations are proportional across the *entire* voltage spectrum. It is often tacitly accepted that in the absence of substrate or presence of inhibitor no current flows through the porter at any voltage. Chapman et al. (1983) have criticized the use of cyanide to extract *dI-V* relations for the *Neurospora* H^+ pump (Gradmann et al., 1978) on this ground, and the same critique applies to analogous studies of *Chara* (Beilby, 1984; Kishimoto et al., 1984; Takeuchi et al., 1985; and *see* Keifer & Spanswick, 1979; Reid & Walker, 1983) and *Riccia*

(Felle, 1981*b*). They note that respiratory blockade can be expected to increase ADP and P_i levels, and promote operation of the transport cycle in the reverse direction. Current subtraction in this instance need not yield a reversal potential (E_{trans}) at all.

The problems associated with characterizing primary proton transport are unique, but the question arises whether similar difficulties might be encountered generally, even when transport activity can be controlled directly through solute additions. This paper examines empirical difference *I-V* methods and the underlying concept of proportional currents as commonly applied in analyzing primary and secondary transport mechanisms. I begin by formulating a set of steady-state kinetic equations which describe *dI-V* relations, and by providing examples of *dI-V* curves under the principle limiting conditions and in relation to several published works. Difference-current-voltage relations can provide kinetic information important in identifying major rate-limiting steps in a transport cycle. I show, too, that current subtractions alone *cannot* yield meaningful reversal potentials under most common experimental conditions.

The Model

Initial Assumptions and the Carrier Model

As a basis for formal treatment, *dI-V* relations can be developed within the context of reaction-kinetic carrier models. I have drawn on the formalism of Hansen et al. (1981) and Sanders et al., (1984), and in keeping with their definitions and conventions I shall limit the discussion to Class I transport mechanisms: those having a single transport loop, in one arm of which the carrier transits the membrane as a charged, and in the other as a neutral species. For the purpose of current-voltage analysis, all such models, regardless of the total number of reaction steps contained, can be reduced to a 2-state form in which all voltage-independent steps are lumped together.

It is from this point that the present discussion will depart. However, a satisfactory treatment of the effects of transport modifiers on *I-V* behavior and *dI-V* characteristics requires that reaction steps directly affected (e.g. in solute binding/debinding) are included in the scheme explicitly. For this purpose the minimum model contains 4 carrier states, which allows for situations in which charge transit steps and the modified (binding/debinding) steps are either adjacent to each other or are separated by intermediate transitions. Interconversions between

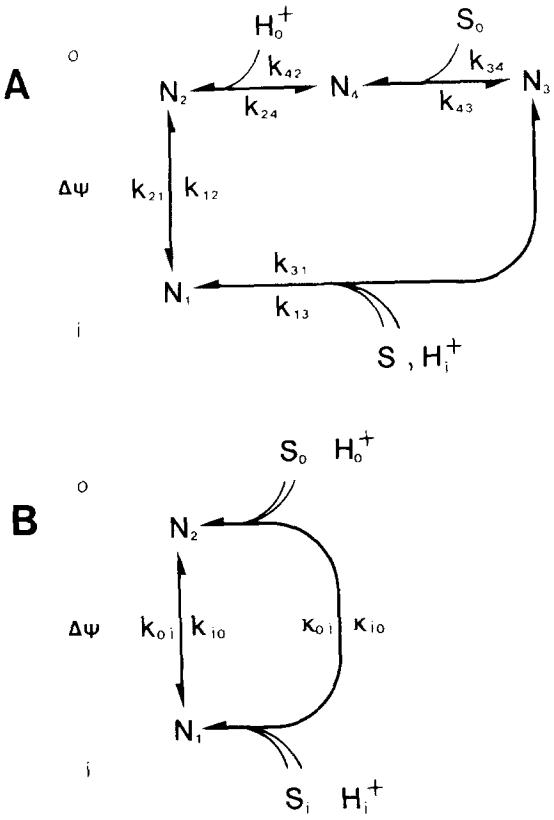

Fig. 1. Models for cotransport of solute (S) with a driver ion (H^+). (*A*) Minimum representation of the carrier cycle with the solute-binding step N_3-N_4 included explicitly, but its kinetic proximity to the charge-transit steps N_2-N_1 undefined. The transition N_1-N_3 subsumes interior solute and driver ion debinding steps and membrane transit of the unloaded carrier. (*B*) Reduced representation of the 4-state model (*A*) with all charge-independent steps lumped in the reaction constants κ_{io} and κ_{oi}

2- and 4-state models (and generally within the family of Class I mechanisms) are facilitated by equivalences of related reaction constants and groups of reaction constants, and present a means to interpreting rate parameters derived empirically from *I-V* and *dI-V* characteristics (*see* Table 1 in Hansen et al., 1981).

Figure 1 illustrates both models in the context of secondary transport coupled to the movement of a driver ion. For the empirical 2-state form, the lumped reaction constants κ_{io} and κ_{oi} subsume binding and debinding steps both for the transported solute and for the driver ion on either side of the membrane. In the 4-state model solute binding and debinding occur in the reaction steps k_{34} and k_{43}, respectively, with external solute concentration appearing explicitly as $k_{34}^o[S]_o(=k_{34})$, where k_{34}^o is the specific reaction rate constant for solute binding ($k_{34}^o = k_{34}$ when $[S]_o = 1$). Membrane transit of the neutral form of the carrier complex, as well as intracel-

lular binding/debinding of solute and driver ion will be treated as constants in the following discussion and are lumped in the reaction constants k_{13} and k_{31}. Exterior driver ion binding/debinding steps, which will also be assumed constant, are included in the lumped rate parameters k_{24} and k_{42}, but again could just as easily be included in the reaction steps between carrier states N_1 and N_3. For situations in which driver ion concentration is varied and solute concentrations remain constant, interpretation of the reaction steps associated with solute and driver ion binding/debinding are simply reversed.

Within the carrier cycles of both models voltage sensitivity is restricted to membrane transit of the charged carrier (Läuger & Stark, 1970). The reaction constants k_{12} and k_{21} for the 4-state model and k_{io} and k_{oi} for the 2-state model incorporate a component for the electric field across the membrane paralleling carrier movement which, as a first approach, will be assigned to a symmetric Eyring barrier within the membrane. Hence, by analogy with the solute binding step, the specific rate constants are defined by

$$k_{12} = k_{12}^o \exp(zu/2), \qquad k_{21} = k_{21}^o \exp(-zu/2) \quad (1a,b)$$

and

$$k_{io} = k_{io}^o \exp(zu/2), \qquad k_{oi} = k_{oi}^o \exp(-zu/2) \quad (2a,b)$$

in which z is the net charge on the carrier during transit and u is the reduced membrane potential, defined as $F\Delta\psi/RT$. (Here F, R and T have their usual meanings. $\Delta\psi$ is taken as the measured membrane potential relative to the cell exterior. The factor 2 places the Eyring barrier symetrically within the membrane.)

In the subsequent discussion it is assumed that the carrier is positively charged when loaded (forward operation of the carrier cycles in Fig. 1 in the counterclockwise direction), but precisely analogous equations and identical results are obtained if the unloaded carrier is assumed to be negatively charged. Likewise, identical arguments can be developed for electrogenic systems which function normally to move positive charge out of the cell. The consequences of current subtraction in the latter case may be seen through symmetry considerations to give results equivalent to those described below, but rotated about the current and voltage axes with respect to the equilibrium potential for charge transit (*see below*).

Formally, all n-state models are derived from the corresponding $n-1$ steady-state rate equations and one equation defining carrier conservation. The ensemble of equations can be expressed in matrix notation (*see* Hansen et al., 1981; Sanders et al., 1984) as

$$\mathbf{M}_n\mathbf{V}_n = N\mathbf{I}_n \quad (3)$$

where N is the total carrier density. For the 4-state model, the matrix $\mathbf{M}_4$ and the vectors $\mathbf{V}_4$, and $\mathbf{I}_4$ are defined by

$$\begin{bmatrix} 1 & 1 & 1 & 1 \\ -(k_{12}+k_{13}) & k_{21} & k_{31} & 0 \\ k_{12} & -(k_{21}+k_{24}) & 0 & k_{42} \\ 0 & k_{24} & k_{34} & -(k_{42}+k_{43}) \end{bmatrix} \cdot \begin{bmatrix} N_1 \\ N_2 \\ N_3 \\ N_4 \end{bmatrix} = N \cdot \begin{bmatrix} 1 \\ 0 \\ 0 \\ 0 \end{bmatrix}. \quad \begin{matrix} (4a) \\ (4b) \\ (4c) \\ (4d) \end{matrix}$$

[The so-called "reserve factors," which bring into account the contributions of unknown intermediate steps in the carrier cycle (Hansen et al., 1981), have been omitted here for clarity. Distortions which unknown steps introduce into the individual reaction constants in practice affect the partitioning of the rate products between the carrier state densities and the reaction constants (*see* Sanders et al., 1984) and are of no consequence to the immediate discussion. I return to the effects of hidden carrier states in relating results obtained below with the 4-state model to those of the empirical 2-state model in which exterior solute binding must be subsumed within the lumped constant κ_{io}.]

The determinant solutions to each of these equations is

$$N_j = |{}^j\mathbf{M}_n|/|\mathbf{M}_n| \quad (5)$$

for $j = 1, 2, \ldots n$ and where $|{}^j\mathbf{M}_n|$ denotes the determinant obtained by substituting the vector $\mathbf{I}_n$ for the jth column of $\mathbf{M}_n$. The steady-state expression for the net current i through the porter is simply the difference between the unidirectional fluxes through the voltage-sensitive arm of the carrier cycle

$$i = zF(k_{12}N_1 - k_{21}N_2) \quad (6)$$

and hence substituting the corresponding carrier state equations (Eq. 5) into Eq. (6) gives

$$i = zFN\,\frac{(k_{12}|{}^1\mathbf{M}_n| - k_{21}|{}^2\mathbf{M}_n|)}{|\mathbf{M}_n|} \quad (7)$$

as the general n-state solution for the *true* steady-state current as a function of voltage. Expanding

this equation yields, for the empirical 2-state form,

$$i = zFN \frac{k_{io}\kappa_{oi} - k_{oi}\kappa_{io}}{k_{io} + k_{oi} + \kappa_{io} + \kappa_{oi}} \tag{8}$$

where the empirical constants k_{io} and k_{oi} are treated equivalently to their n-state counterparts k_{12} and k_{21}. For the 4-state model Eq. (7) yields

$$i = zFN \frac{k_{12}k_{24}k_{43}k_{31} - k_{21}k_{13}k_{34}k_{42}}{\begin{aligned} &k_{21}k_{42}(k_{34} + k_{31}) + k_{31}k_{43}(k_{24} + k_{21}) \\ &+ k_{12}k_{31}(k_{43} + k_{42}) + k_{42}k_{34}(k_{13} + k_{12}) \\ &+ k_{13}k_{21}(k_{42} + k_{43}) + k_{43}k_{24}(k_{12} + k_{13}) \\ &+ k_{24}k_{12}(k_{31} + k_{34}) + k_{34}k_{13}(k_{21} + k_{24}) \end{aligned}}. \tag{9}$$

The Consequence of Current Subtraction

In formulating *difference* current equations for n-state models, precisely the same strategy is followed as is applied experimentally. Accordingly, I have made the following assumptions: (i) Under all experimental conditions considered the transport system is at steady-state ($dN_j/dt = 0$). (ii) The total amount of carrier within the cycle remains constant. (iii) All reaction steps are physically discrete, and experimental changes in membrane potential and solute concentration outside affect only those steps directly involved in membrane charge transit and solute binding, respectively. (iv) The net steady-state current across the membrane unrelated to the transport system remains constant at all voltages.

Assumptions (i) and (ii) are normally met in practice when current measurements (under voltage clamp) are carried out over tens or hundreds of milliseconds, and when the interval between successive clamp cycles (with/without added solute) is short. The third assumption is the simplest conceptually in which to view effects of varying "substrate" (solute and membrane potential) conditions for the porter. The fourth assumption ensures that *dI-V* relations obtained by current subtraction are consequent solely of changes in transporter currents (*see* Introduction), and for computational purposes means that the *I-V* relations of the porter only need be considered.

Current subtraction, then, implies that at every membrane potential the net transporter-specific difference current

$$\Delta i = i^+ - i^- \tag{10}$$

where the superscripts $-$ and $+$ will be used to denote the conditions without and with added solute, respectively. Substituting Eq. (7) into the right-hand side and rearranging terms then gives

$$\Delta i = zFN \frac{\begin{aligned} &k_{12}\{|{}^1\mathbf{M}_n^+||\mathbf{M}_n^-| - |{}^1\mathbf{M}_n^-||\mathbf{M}_n^+|\} \\ &+ k_{21}\{|{}^2\mathbf{M}_n^-||\mathbf{M}_n^+| - |{}^2\mathbf{M}_n^+||\mathbf{M}_n^-|\} \end{aligned}}{|\mathbf{M}_n^+||\mathbf{M}_n^-|} \tag{11}$$

as the general solution for the difference current for all n-state formulations. Sadly, the significance of Eq. (11) is not immediately evident, but it can be summarized verbally. The denominator is the sum of n^4 terms, including terms containing $[S]_o^-$ and $[S]_o^+$, and each term is the product of $2(n-1)$ reaction constants. In the numerator all cross products (exactly half) cancel, except those which carry a positive sign and include the term $[S]_o^-$ and those which carry a negative sign and include the term $[S]_o^+$. As a result, the quantity $([S]_o^- - [S]_o^+)$ factors out leaving, in the numerator, the sum of n^2 terms where, again, each term is the product of $2(n-1)$ reaction constants. Expansion of Eq. (11) thus yields for the empirical 2-state model

$$\Delta i = zFN(\kappa_{io}^- - \kappa_{io}^+) \frac{\begin{aligned} &k_{oi}^{o2}\exp(-zu) + k_{io}^o\exp(zu/2)\kappa_{oi} \\ &+ k_{oi}^o\exp(-zu/2)\kappa_{oi} + k_{io}^o k_{oi}^o \end{aligned}}{|\mathbf{M}_2^-||\mathbf{M}_2^+|} \tag{12a}$$

where

$$\begin{aligned} |\mathbf{M}_2^-||\mathbf{M}_2^+| = {} & k_{io}^{o2}\exp(zu) + k_{oi}^{o2}\exp(-zu) \\ & + k_{io}^o\exp(zu/2)(2\kappa_{oi} + \kappa_{io}^- + \kappa_{io}^+) \\ & + k_{oi}^o\exp(-zu/2)(2\kappa_{oi} + \kappa_{io}^- + \kappa_{io}^+) + 2k_{io}^o k_{oi}^o \\ & + \kappa_{oi}(\kappa_{io}^- + \kappa_{io}^+) + \kappa_{io}^+\kappa_{io}^- + \kappa_{oi}^2 \end{aligned} \tag{12b}$$

and for the 4-state model

$$\Delta i = zFNk_{34}^o([S]_o^- - [S]_o^+) \frac{\begin{aligned} &k_{24}k_{43}k_{31}\{k_{12}^{o2}\exp(zu)(k_{24} + k_{42}) \\ &+ k_{12}^o\exp(zu/2)k_{13}(k_{24} + k_{42}) + k_{12}^o k_{21}^o(k_{13} + k_{42})\} \\ &+ k_{13}k_{42}\{k_{21}^{o2}\exp(-zu)(k_{13} + k_{31})(k_{43} + k_{42}) \\ &+ k_{21}^o\exp(-zu/2)k_{24}k_{43}(k_{13} + k_{31}) \\ &+ k_{21}^o k_{12}^o(k_{31}(k_{43} + k_{42} + k_{24}) + k_{43}k_{24})\} \end{aligned}}{|\mathbf{M}_4^-||\mathbf{M}_4^+|} \tag{13a}$$

where

$$|\mathbf{M}_4^-| = k_{12}^o \exp(zu/2)\{[S]_o^- k_{34}^o(k_{24} + k_{42}) + k_{31}(k_{43} + k_{42} + k_{24}) + k_{43}k_{24}\} + k_{21}^o \exp(-zu/2)\{[S]_o^- k_{34}^o (k_{42} + k_{13}) + (k_{43} + k_{42})(k_{13} + k_{31})\} + [S]_o^- k_{34}^o k_{13} (k_{24} + k_{42}) + k_{43}k_{24}(k_{13} + k_{31}) \quad (13b)$$

$$|\mathbf{M}_4^+| = k_{12}^o \exp(zu/2)\{[S]_o^+ k_{34}^o(k_{24} + k_{42}) + k_{31}(k_{43} + k_{42} + k_{24}) + k_{43}k_{24}\} + k_{21}^o \exp(-zu/2)\{[S]_o^+ k_{34}^o (k_{42} + k_{13}) + (k_{43} + k_{42})(k_{13} + k_{31})\} + [S]_o^+ k_{34}^o k_{13} (k_{24} + k_{42}) + k_{43}k_{24}(k_{13} + k_{31}) \quad (13c)$$

and the voltage (exponential) terms are now included explicitly.

Since the ratio of the sums and products of the rate constants will always be a positive value (and remembering that $z > 0$), it is clear that the sign of the resulting *difference* current must depend on the factor $([S]_o^- - [S]_o^+)$. In other words, *current subtractions carried out under conditions in which solute concentration [or more generally, in which the transport cycle (see above)] is modified asymmetrically yields an apparent inward (negative) current at all finite membrane potentials.* As a corollary to this conclusion, it is clear that any attempt to determine the reversal potential for a transport system by seeking the point at which the *dI-V* curve *crosses* the voltage axis will de doomed to failure or, worse still, may give wholly erroneous results. These points will be taken up in greater depth in the Examples and Discussion below.

Identifying Rate-Limiting Steps in a Reaction Cycle

While current subtraction cannot be expected to give meaningful transport reversal potentials when the thermodynamic constraints on transport are affected, *dI-V* relations are capable of providing information as to the dominant rate-limiting reaction sequence(s) in the carrier cycle. I examine the primary characteristics associated with *dI-V* curves in this section. Additional features are introduced in the Examples.

The most obvious characteristic exhibited by *dI-V* curves relates to the relative rates of the charge-dependent *vs.* charge-independent reactions. To illustrate this point it is necessary to examine the slope, or "conductance," of the *dI-V* curve. [Normally conductance has a precise physical meaning (in simplest terms, equivalent to $1/R$, where R is electrical resistance) related to the movement of charge through a membrane or porter. This meaning is lost in the context of current subtraction, but I shall retain the term, denoted as $\bar{g}$, with reference to the empirically derived relationships.] Now, an important prediction of Class I transport mechanisms (and indeed of any transport model which shows current saturation at voltage extremes) is the occurrence of a single or of paired conductance maxima in the transporter conductance-voltage curve. Beilby illustrates this prediction and two possible outcomes for hypothetical *I-V* curves (1984, Fig. 13), and similar *g-V* relations can be visualized by mentally plotting, as a function of voltage, the instantaneous slopes for the hypothetical *I-V* curves published in Hansen et al. (1981, Fig. 5). The number (1 or 2) of conductance maxima reflects the number of "bends" in the *I-V* curve, which in turn depends on the relative rates of reaction steps in the charge-dependent and charge-independent arms of the carrier cycle. In general, when the inequality

$$(k_{io}^o k_{oi}^o)^{1/2} \gg \kappa_{io} + \kappa_{oi} \quad (14)$$

holds, the *I-V* curve behaves as a simple hyperboloic tangent function and gives a single conductance maximum only; when the inequality fails (membrane charge transit slow in relation to binding/debinding steps and uncharged carrier transit) the slope of the *I-V* curve drops at voltages near the reversal potential for the voltage-sensitive limb of the reaction cycle ($=E_c$, *see below*) and two conductance peaks may be observed.

An analogous set of criteria applies to $\bar{g}$-*V* relations, with the distinction that *dI-V* derived conductances may drop *below* zero when the inequality (14) does not hold. Several of the $\bar{g}$-*V* relations included with each of the examples below exhibit this behavior, and a formal demonstration follows. The conductance $\bar{g}$ is obtained by differentiating Eq. (12) with respect to $\Delta\psi$, and after rearranging terms gives

$$\bar{g} = \frac{z^2F^2N(\kappa_{io}^+ - \kappa_{io}^-)}{2RT} \cdot \frac{K}{(|\mathbf{M}_2^-||\mathbf{M}_2^+|)^2} \quad (15a)$$

where $|\mathbf{M}_2^-||\mathbf{M}_2^+|$ is defined by the identity (12b) and

$$K = k_{io}^{o3} \exp(3zu/2)\kappa_{oi} + 2k_{io}^{o3}k_{oi}^o \exp(zu) + \exp(zu/2)\{k_{io}^{o2}k_{oi}^o(3\kappa_{oi} + \kappa_{io}^- + \kappa_{io}^+) - k_{io}^o(\kappa_{oi}^3 + \kappa_{oi}^2(\kappa_{io}^- + \kappa_{io}^+) + \kappa_{oi}\kappa_{io}^+\kappa_{io}^-)\} + k_{oi}^{o3} \exp(-3zu/2)(\kappa_{oi} + \kappa_{io}^- + \kappa_{io}^+) + 2\exp(-zu)\{k_{oi}^{o3}k_{io}^o + k_{oi}^{o2}(\kappa_{oi}(\kappa_{io}^- + \kappa_{io}^+) + \kappa_{io}^-\kappa_{io}^+ + \kappa_{oi}^2)\} + \exp(-zu/2)\{2k_{oi}^{o2}k_{io}^o(\kappa_{oi} + \kappa_{io}^- + \kappa_{io}^+) + k_{oi}^o(\kappa_{oi}^3 + \kappa_{oi}^2(\kappa_{io}^- + \kappa_{io}^+) + \kappa_{oi}\kappa_{io}^+\kappa_{io}^-)\} + 4k_{io}^{o2}k_{oi}^{o2}. \quad (15b)$$

Again the exponential (voltage) terms are included explicitly for clarity. Notice that the difference in κ_{io} now carries a positive sign. When κ_{io} and κ_{oi} are very small [so that $(k^o_{io}k^o_{oi})^{1/2} \gg \kappa_{io} + \kappa_{oi}$] all products of these constants drop out. Equation (15) then simplifies to

$$\bar{g} = \frac{z^2F^2N(\kappa^+_{io} - \kappa^-_{io})}{RT} \frac{k^{o3}_{io}k^o_{oi}\exp(zu) + k^o_{io}k^{o3}_{oi}\exp(-zu) + 2k^{o2}_{io}k^{o2}_{oi}}{(k^o_{io}\exp(zu/2) + k^o_{oi}\exp(-zu/2))^4} \quad (16)$$

for which the ratio of the reaction constants equals $\frac{1}{4}$ and $\bar{g} = \bar{g}_{max}$, the conductance maximum, when

$$\exp(zu) = k^o_{oi}/k^o_{io} \text{ or } \Delta\psi = E_c = \frac{RT}{zF}\ln(k^o_{oi}/k^o_{io}) \quad (17)$$

and goes to 0 at large positive and negative voltages. Hence $\bar{g}_{max}$ in this case also identifies the empirical ratio k^o_{oi}/k^o_{io}.

The identities of Eq. (17) define the reversal potential for the voltage-sensitive limb of the reaction cycle (E_c, Hansen et al., 1981) and have a particular significance for *dI-V* relations which I take up shortly. For the moment, they allow the axial transformation

$$u = v + \frac{zF}{RT}E_c. \quad (18)$$

Now in the other limiting case, when κ_{io} and κ_{oi} are large [$(k^o_{io}k^o_{oi})^{1/2} \not\gg \kappa_{io} + \kappa_{oi}$], and for potentials near 0 ($v \approx -zFE_c/RT$, or $\Delta\psi \approx E_c$), Eq. (15) reduces to

$$\bar{g} = \frac{z^2F^2N(\kappa^+_{io} - \kappa^-_{io})}{2RT} \cdot \frac{k^o_{oi}C\exp(-zu/2) - k^o_{io}\exp(zu/2)}{(|\mathbf{M}^-_2||\mathbf{M}^+_2|)^2} \quad (19a)$$

where

$$C = \kappa^3_{oi} + \kappa^2_{oi}(\kappa^-_{io} + \kappa^+_{io}) + \kappa_{oi}\kappa^+_{io}\kappa^-_{io}. \quad (19b)$$

In this case, the ratio of reaction constant sums and products, and hence $\bar{g}$, equals zero when $u = 0$ ($\Delta\psi = E_c$), carries a negative sign at positive potentials and a positive sign at negative potentials. Now, it is the $\bar{g}$-V inflection point which identifies the empirical ratio k^o_{oi}/k^o_{io}.

Current subtractions, in many cases, should also permit an estimate for the empirical constant κ_{io}. For saturating negative voltages Eq. (12) reduces to

$$\Delta i = \Delta i_{-sat} = zFN(\kappa^-_{io} - \kappa^+_{io}) \quad (20)$$

which, for small values of κ^-_{io}, approximates the true transporter current at saturating negative voltages, i_{-sat} (*see* Hansen et al., 1981). In this context, it is worth noting that i_{+sat} ($=zFN\kappa_{oi}$), the transporter current at saturating positive voltages, has no equivalent in *dI-V* relations. From Eq. (12) it can be seen that at large positive voltages $\Delta i_{+sat} = 0$. A similar set of relationships can be derived from Eqs. (9) and (13), in which case

$$i_{+sat} = zFN \frac{k_{24}k_{43}k_{31}}{k_{34}(k_{24} + k_{13}) + k_{31}(k_{24} + k_{42} + k_{43}) + k_{24}k_{43}} \quad (21)$$

$$i_{-sat} = -zFN \frac{k_{13}k_{34}k_{42}}{k_{34}(k_{42} + k_{13}) + (k_{42} + k_{43})(k_{13} + k_{31})} \quad (22)$$

and, for $[S]^-_o \approx 0$, the difference currents at saturating voltages

$$\Delta i_{+sat} = -zFN \frac{k_{24}k_{43}k_{31}}{k_{31}(k_{43} + k_{42} + k_{24}) + k_{43}k_{24} + \dfrac{(k_{31}(k_{43} + k_{42} + k_{24}) + k_{43}k_{24}}{[S]^+_o k^o_{34}(k_{42} + k_{24})}} \quad (23)$$

$$\Delta i_{-sat} = -zFN \frac{k_{13}k_{42}}{k_{42} + k_{13} + \dfrac{(k_{13} + k_{31})(k_{43} + k_{42})}{[S]^+_o k^o_{34}}}. \quad (24)$$

Including solute binding explicitly shows that circumstances can be found in which Δi_{+sat} is nonzero. Note that both at negative *and* at positive saturating voltages the difference currents nonetheless carry a negative sign.

It is also of some interest that Eqs. (23), (24),

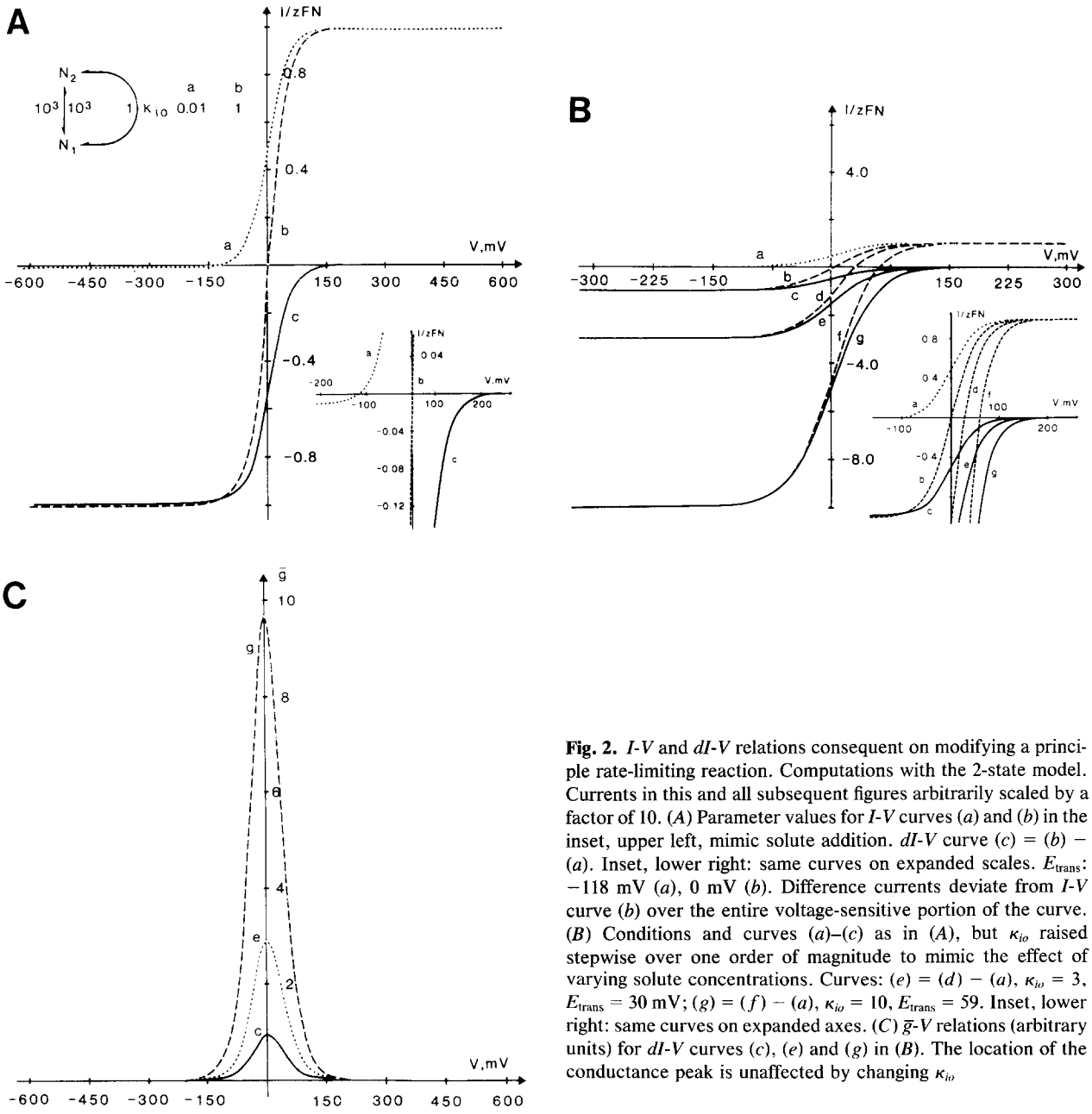

Fig. 2. *I-V* and *dI-V* relations consequent on modifying a principle rate-limiting reaction. Computations with the 2-state model. Currents in this and all subsequent figures arbitrarily scaled by a factor of 10. (*A*) Parameter values for *I-V* curves (*a*) and (*b*) in the inset, upper left, mimic solute addition. *dI-V* curve (*c*) = (*b*) − (*a*). Inset, lower right: same curves on expanded scales. E_{trans}: −118 mV (*a*), 0 mV (*b*). Difference currents deviate from *I-V* curve (*b*) over the entire voltage-sensitive portion of the curve. (*B*) Conditions and curves (*a*)–(*c*) as in (*A*), but κ_{io} raised stepwise over one order of magnitude to mimic the effect of varying solute concentrations. Curves: (*e*) = (*d*) − (*a*), κ_{io} = 3, E_{trans} = 30 mV; (*g*) = (*f*) − (*a*), κ_{io} = 10, E_{trans} = 59. Inset, lower right: same curves on expanded axes. (*C*) $\bar{g}$-*V* relations (arbitrary units) for *dI-V* curves (*c*), (*e*) and (*g*) in (*B*). The location of the conductance peak is unaffected by changing κ_{io}

and indeed Eq. (13), include terms with $[S]_o$ in the denominator. Minor rearrangements of Eqs. (23) and (24), and more lengthy algebraic manipulation of Eq. (13), result in the familiar Michaelis-Menten formulation where, in this case, $\Delta i = -\Delta I_{max}[S]_o/([S]_o + K_m)$, and ΔI_{max} and K_m are sums, products and ratios of reaction constants. It follows that difference currents measured at *any* one membrane potential will behave in a 'sensible' and simple Michaelian fashion, regardless of the voltage displacement from E_{trans}. This point is, in fact, a restatement of the previous conclusion that in the difference currents kinetic behavior alone—now with respect to the *chemical* parameters—will not reveal the thermodynamic constraints on the porter.

Examples

Numerical Considerations

In assigning numerical values to the reaction constants for each of the examples below, I have placed no restrictions on the site(s) of energetic transitions.

This accords with Hill and Eisenberg's (1981) proposal that such transitions may be dissociated from solute passage through the reaction cycle. The only stipulation was that at equilibrium the ratio of the products of forward and reverse reaction constants was equal to 1. In addition I began, by analogy to several known transporters and common experimental situations (Belkhode & Scholefield, 1969; Hajjar et al., 1970; Pall, 1971; Morrison & Lichtstein, 1976; Giaquinta, 1980; Sanders; 1980*a*,*b*; Sanders & Hansen, 1981; Blatt et al., 1984; Lass & Ullrich-Eberius, 1984; Ullrich-Eberius et al., 1984; Rodriguez-Narvarro & Ramos, 1984; Rodriguez-Navarro et al., 1986), with the understanding that $[S]_i$ is finite (if small) and that $[S]_i \gg [S]_o$ in the absence of added solute—in other words, that the transport system is not irreversible at all membrane potentials. Finally, for all of the examples below the valence, $z = 1$. Similar results can be obtained for higher valencies; only the voltage spread is compressed (by the factor z).

For consistency between sets of computations, the reaction constants for each example were poised initially to give $E_{trans} = -120$ mV and $[S]_o$ (κ_{io} or k_{34}) was then increased 100-fold ($E_{trans} = 0$ mV), or more in some cases. Otherwise, as much as possible individual reaction constants were set to unity for ease in computation. (The absolute values of the individual constants chosen in no way affect the features of the resulting *dI-V* relations, except as scalars; rather, it is the relative value of each constant in relation to the others, and the manner in which these relations change which dictate the outcome.) Most computations were carried out with the aid of a microcomputer. Equations (8), (9), (12) and (13) were used to generate the *I-V* and *dI-V* curves. $\bar{g}$-*V* relations were obtained by Lagrangian interpolation and differentiation.

Solute Addition Modifies a Rate-Limiting Reaction

The simplest case occurs when membrane transit of the charged carrier is rapid compared with all other reaction steps $[(k^o_{io}k^o_{oi})^{1/2} \gg \kappa_{io} + \kappa_{oi}]$. The transporter *I-V* relations follow single hyperbolic tangent functions and the difference currents mirror this behavior below the voltage axis. The curves in Fig. 2*A* and 2*B* were calculated using the empirical 2-state model. The 'control' ($[S]^-_o$, dotted line) and 'plus solute' ($[S]^+_o$, dashed lines) *I-V*, and *dI-V* (solid lines, =dashed lines − dotted line) characteristics for each computation are shown. Under these conditions Eq. (12) reduces to

$$\Delta i = zFN(\kappa^-_{io} - \kappa^+_{io}) \cdot \frac{k_{oi}}{k_{io} + k_{oi}} \tag{25}$$

which goes to $zFN(\kappa^-_{io} - \kappa^+_{io})$ and zero monotonically at infinite negative and positive membrane potentials, respectively.

Two additional features are apparent in *dI-V* curves described by Eq. (25). First, the half-maximal difference current, $\Delta i_{1/2} = zFN(\kappa^-_{io} - \kappa^+_{io})/2$, occurs when $\Delta\psi = E_c$ (Eq. 17). The peak conductance, $\bar{g}_{max}$, occurs at this potential as well (Eqs. (16), (17) and Fig. 2*C*). E_c thus establishes the axial (voltage) symmetry for the *dI-V* characteristic. Significantly, the voltage symmetry is independent of changes in the reaction constants κ_{io} and κ_{oi}. As a result, modifying κ_{io} (and in most cases $[S]_o$, but *see below*) over a range of values yields a family of *dI-V* curves which, on appropriate scaling with respect to the current axis, are superimposable (*see* Fig. 2*B*). In other words, the *voltage displacement of the dI-V curve is independent of the choices for* $[S]_o$ *and* $([S]^+_o - [S]^-_o)$.

The second feature of curves in this category relates to the slope and spread of voltage-dependent regions in *dI-V* relations. From Eq. (16), the peak conductance reduces to

$$\bar{g}_{max} = \frac{z^2F^2N(\kappa^+_{io} - \kappa^-_{io})}{4RT} \tag{26}$$

which gives a (peak) slope conductance of $zFN(\kappa^+_{io} - \kappa^+_{io})/2(=\Delta i_{1/2})$ per 51 mV for $z = 1$. The same conclusion can be drawn from Eqs. (24)–(27) of Hansen et al. (1981) which, together with Eq. (18) and the axial translation

$$i = I - \Delta i_{1/2}, \tag{27}$$

also give the characteristic voltage displacement required to give a half-maximal displacement of the difference current from $\Delta i_{1/2}$

$$(\Delta\psi - E_c) = 28/z \text{ (in mV)}. \tag{28}$$

Precisely the same relationship is obtained for half-saturating currents in the *I-V* characteristics (Eq. (28), Hansen et al., 1981) and the same tests, applied to the *I-V* relations, may be adopted now for the difference currents. Hence, if $\bar{g}_{max}$ approximates $\Delta i_{1/2}$ per 51 mV, Eqs. (16), (25) and (26) apply and $z = 1$. Higher conductances require greater charge stoichiometries, and appreciably lower conductances imply that the initial assumption $(k^o_{io}k^o_{oi})^{1/2} \gg \kappa_{io} + \kappa_{oi}$ is not valid. Of course, these distinctions can be made only if *dI-V* relations exhibit a region of voltage sensitivity and Δi_{-sat} is known.

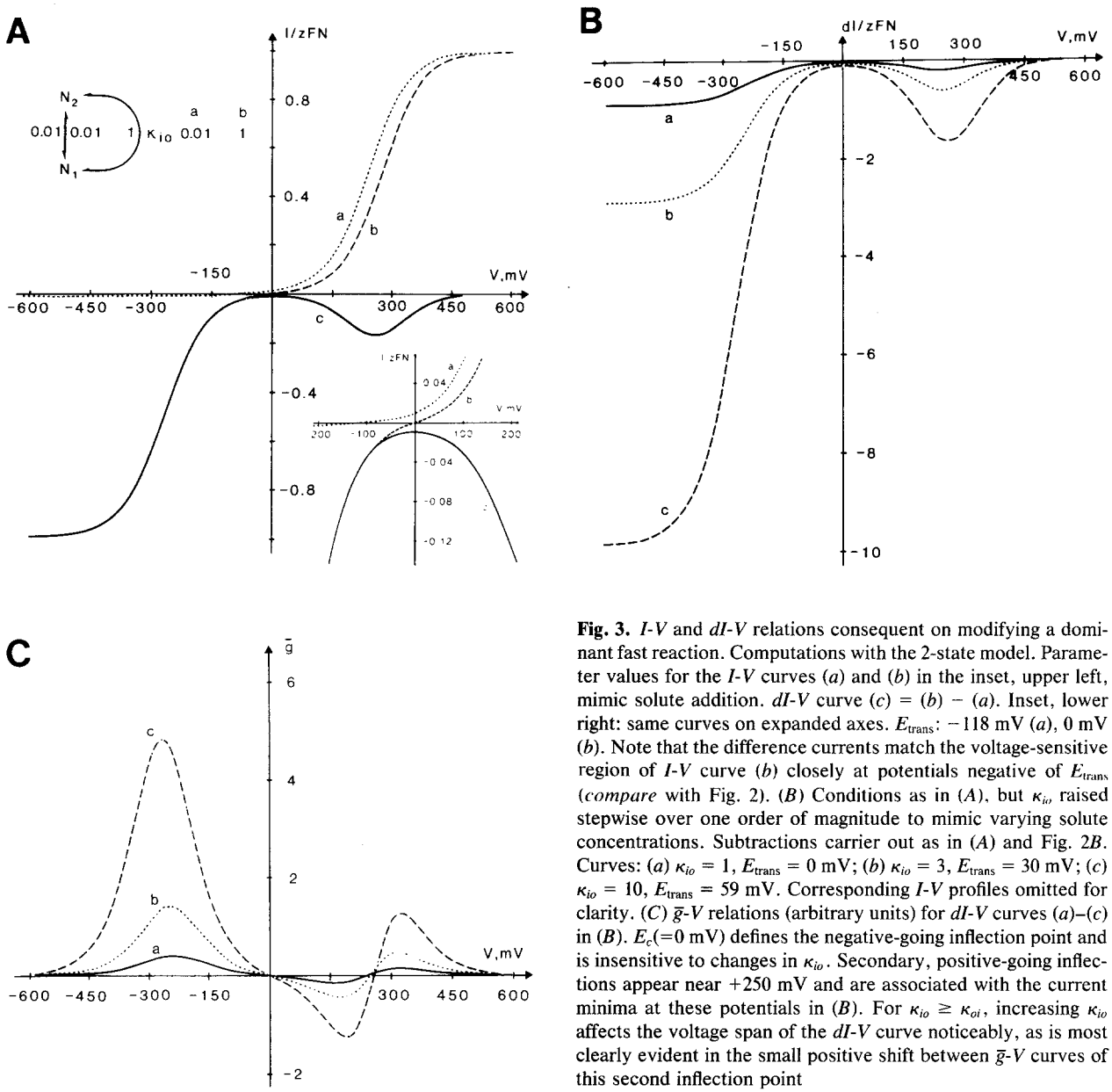

Fig. 3. *I-V* and *dI-V* relations consequent on modifying a dominant fast reaction. Computations with the 2-state model. Parameter values for the *I-V* curves (*a*) and (*b*) in the inset, upper left, mimic solute addition. *dI-V* curve (*c*) = (*b*) − (*a*). Inset, lower right: same curves on expanded axes. E_{trans}: −118 mV (*a*), 0 mV (*b*). Note that the difference currents match the voltage-sensitive region of *I-V* curve (*b*) closely at potentials negative of E_{trans} (*compare* with Fig. 2). (*B*) Conditions as in (*A*), but κ_{io} raised stepwise over one order of magnitude to mimic varying solute concentrations. Subtractions carrier out as in (*A*) and Fig. 2*B*. Curves: (*a*) κ_{io} = 1, E_{trans} = 0 mV; (*b*) κ_{io} = 3, E_{trans} = 30 mV; (*c*) κ_{io} = 10, E_{trans} = 59 mV. Corresponding *I-V* profiles omitted for clarity. (*C*) $\bar{g}$-*V* relations (arbitrary units) for *dI-V* curves (*a*)–(*c*) in (*B*). E_c(=0 mV) defines the negative-going inflection point and is insensitive to changes in κ_{io}. Secondary, positive-going inflections appear near +250 mV and are associated with the current minima at these potentials in (*B*). For $\kappa_{io} \geq \kappa_{oi}$, increasing κ_{io} affects the voltage span of the *dI-V* curve noticeably, as is most clearly evident in the small positive shift between $\bar{g}$-*V* curves of this second inflection point

One additional point bears mentioning. As an inspection of Fig. 2*A* and 2*B* shows, *dI-V* curves of this type will invariably overestimate (toward more positive potentials) the true E_{trans} when extrapolated to the voltage axis. (For a primary electrogenic system operating to move positive charge out of a cell the sign of the error is reversed.) Of course, as the *true* positive saturation current for the porter decreases ($\kappa_{io}^{+} \gg \kappa_{oi}$) extrapolations of difference current relations will approach the true E_{trans}.

Solute Addition Modifies a Dominant Fast Reaction

The second limiting case arises when binding, debinding and uncharged carrier transit steps are rapid compared with membrane transit of the charged carrier [$(k_{io}^{o}k_{oi}^{o})^{1/2} \gg \kappa_{io} + \kappa_{oi}$]. Then *dI-V* characteristics can reveal a second region of negative (inward-going) current, as shown in Fig. 3*A* between *ca.* 100 and 400 mV. Conductance-voltage relations now *cross* the voltage axis, going positive to negative with increasing (more positive) $\Delta\psi$, when $\Delta\psi = E_c$ (Eq. 19). Again, E_c determines the voltage symmetry for the difference currents, and the voltage displacement of the *dI-V* profile is largely independent of κ_{io} (Figs. 3*B*,*C*).

Intermediate situations, too, are easily found, some of which are illustrated in Fig. 4*A*,*B*. A sharp transition occurs over a narrow range of values for the ratio $r = (\kappa_{io} + \kappa_{oi})/(k_{io}^{o}k_{oi}^{o})^{1/2}$ when the $\bar{g}$-*V* characteristic passes from a simple bell shape to curves

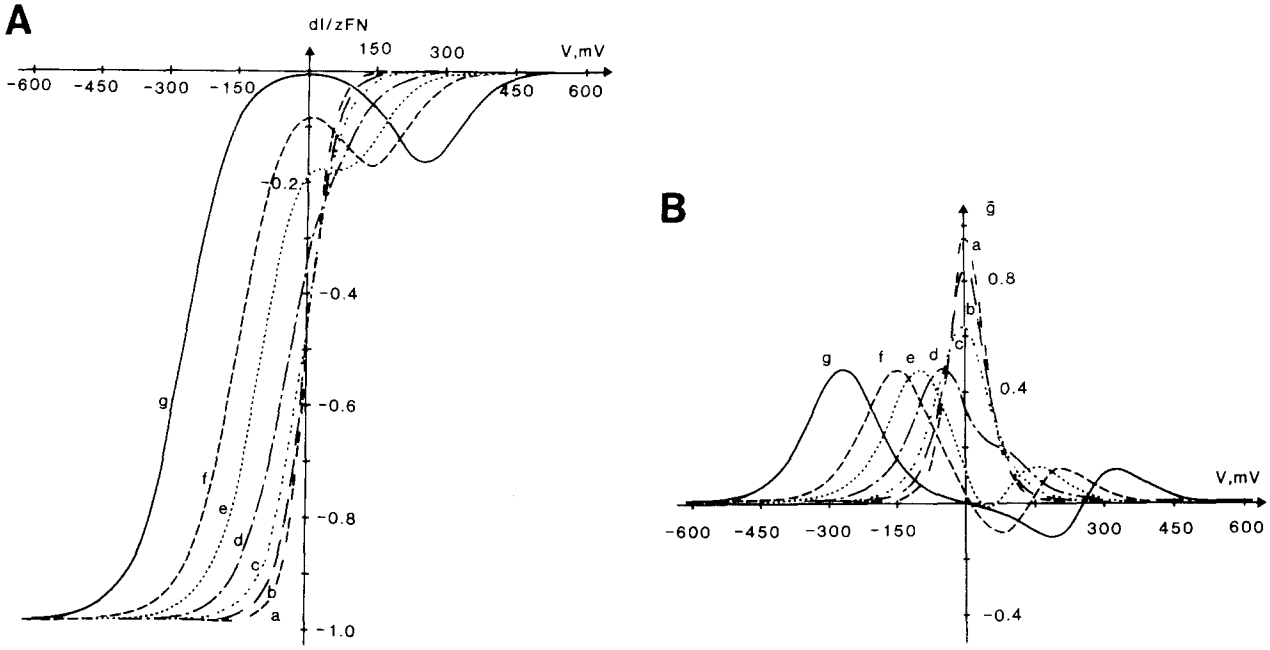

Fig. 4. *dI-V* dependence on the relative rates of charge-dependent and charge-independent transitions. Computations with the 2-state model. Conditions as in Figs. 2*A* and 3*A*, except that k^o_{io} and k^o_{oi} are varied over 4 orders of magnitude as listed in the Table. *dI-V* (*A*) and corresponding $\bar{g}$-*V* (*B*) curves show a marked transition when $(k^o_{io}k^o_{oi})^{1/2} \approx \kappa_{io} + \kappa_{oi}$. Conductances plotted in arbitrary units

in which $\bar{g}$ drops below zero (*see* Fig. 4*A*,*B* and Table). Numerical treatments also indicate that for $r \gg 1$, a 10-fold increase in r is accompanied by an increase in the conductance peak-to-peak (positive-negative) voltage spread, $\bar{s} = 4u/z$ (*see* Table). In practical terms, when $r = 100$ and $z = 1$ the principle voltage-dependent features in the difference currents are spread over *more than 600 mV*.

Equations (12) and (15) and the curves illustrated in Figs. 2–4 approximate *dI-V* behavior for Class I transport systems as long as the carrier bulk resides in states defined by $N_1 + N_2$. A broader range of *dI-V* curve shapes can be accommodated, however, when solute binding and debinding steps, and additional carrier states, are included explicitly. The remaining examples described below examine in greater depth primarily those situations in which k^o_{io} and k^o_{oi} (specifically, their n-state equivalents k^o_{12} and k^o_{21}) are not large. Following Table 2 of Hansen et al. (1981) as a guide to limiting situations, I have selected four of the most interesting cases which illustrate the qualitative scope of *dI-V* profiles beyond those in Figs. 2–4, and which have important experimental implications. As will be seen shortly, only under restricted conditions is it reasonable to assume, as I have above, that the empirical reaction constant κ_{io} alone is affected by external solute changes.

In each case, I began with the reaction constants poised so that on 'adding' solute (and for $\Delta\psi = E_c$) the bulk of the carrier was distributed symmetrically about the solute binding step. (Shifting the carrier bulk away from the carrier states N_1 and N_2 associated directly with membrane charge transit introduces additional states functionally into the reaction cycle.) Then by altering subsets of reaction constants while maintaining E_{trans} 'plus solute' and the change in k_{34} $[=([S]^+_o - [S]^-_o)k^o_{34}]$ constant for each *dI-V* curve, it was possible to shift the carrier distribution between selected states and thereby construct sets of related curves. This approach had

Table. *dI-V* parameter dependence on inherent rates of charge-sensitive *vs.* charge-insensitive reactions[a]

Curve	k^o_{io}, k^o_{oi}	r	$\bar{s}$
a	1000	0.002	—
b	10	0.2	—
c	3	0.67	—
d	1	2.0	—
e	0.3	6.67	142
f	0.1	20	236
g	0.01	200	472
h[b]	0.001	2000	708

[a] Data for the curves in Fig. 4*A* and 4*B*. κ_{io}, $\kappa_{oi} = 1$ ('plus solute') and $k^o_{io} = k^o_{oi}$ throughout. Parameters r and $\bar{s}$, defined in the text, provide convenient indices to the relative rates of charge-sensitive and -insensitive carrier transitions, and to the voltage-sensitive span of the *dI-V* relations, respectively. $\bar{s}$ was determined here, and in all subsequent figures, by numerical differentiation of the $\bar{g}$-*V* relations.

[b] Curve not shown in Fig. 4.

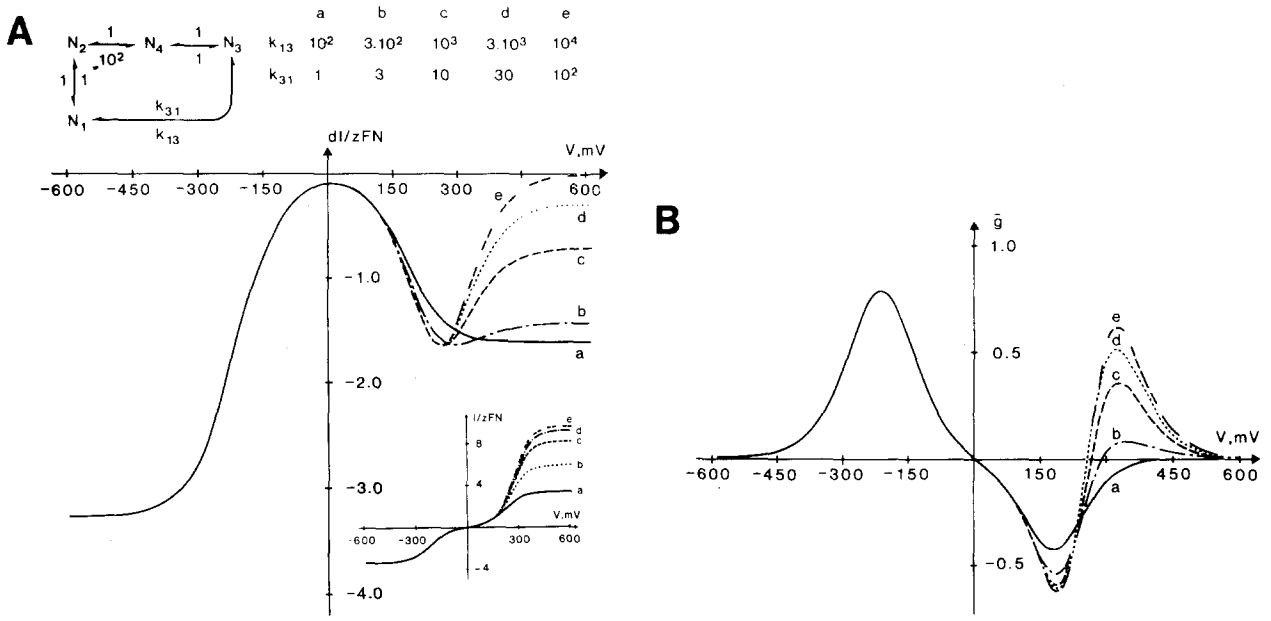

Fig. 5. *I-V* and *dI-V* dependence on membrane transit of the uncharged carrier. k_{13} and k_{31} increased in parallel over 2 orders of magnitude. (*A*) *dI-V* curves with parameter values as shown in the inset, upper left. Inset, lower right: corresponding 'plus solute' *I-V* curves. For $k_{31} > k_{34}$ the *dI-V* relations recurve toward the voltage axis at large positive potentials. [Decreasing k_{13} and k_{31} reduces Δi_{+sat} in relation to curve (*a*) without a qualitative change in the *dI-V* profile (*not shown*).] Note that Δi_{+sat} and i_{+sat} are affected inversely. (*B*) Corresponding $\bar{g}$-*V* curves (arbitrary units) showing the resultant secondary inflection point (*compare* with Fig. 3*C*). No effect either on E_c or on the *dI-V* voltage-sensitive span ($\bar{g}$-*V* maximum-minimum span $\bar{s}$ = 405 mV, between *ca.* −200 and +200 mV) is evident

the effect of scaling results within each set of curves and between sets for comparing the changes both in *I-V* and *dI-V* relations. (The same operation was carried out in deriving the curves in Fig. 4. It should be recognized that the *families* of *I-V* and *dI-V* relations illustrated in Fig. 5–8, as in Fig. 4, are not the consequence of sequential solute 'additions,' but might be observed only on introducing a third experimental dimension such as modulating trans-ligand concentrations.)

Proximity of Membrane Charge Transit to Solute Debinding

The outcome of parallel changes in the lumped reaction constants k_{13} and k_{31} are shown in Fig. 5. Increasing the rate of carrier recycling (and binding/debinding on the membrane interior) has the effect of increasing i_{+sat} in the *I-V* while decreasing Δi_{+sat} in the *dI-V* relations of the porter. No change is observed either in i_{-sat} or in Δi_{-sat}. Since in this case, $k_{24} \gg k_{42}$ and the relationship $k_{13} \gg k_{31}$, k_{42}, k_{43}, $[S]_o k^o_{34}$ is retained while k_{31} becomes very large in relation to $[S]_o k^o_{34}$ and k_{43}, for the porter *I-V* relations Eqs. (21) and (22) reduce to

$$i_{+sat} = zFN \frac{k_{43}}{1 + (k_{43} + k_{34})/k_{31}},$$

$$i_{-sat} = zFN \frac{k_{42}}{1 + ((k_{42} + k_{43})/k_{34})(1 + k_{31}/k_{13})} \quad (29a,b)$$

and for the *dI-V* characteristic Eqs. (23) and (24) simplify to

$$\Delta i_{+sat} = -zFN \frac{k_{43}}{1 + k_{31}/[S]^+_o k^o_{34}},$$

$$\Delta i_{-sat} = -zFN \frac{k_{42}}{1 + (k_{43} + k_{42})/[S]^+_o k^o_{34}}. \quad (30a,b)$$

Hence, both i_{-sat} and Δi_{-sat} remain independent of k_{13} and k_{31} (in the former case, as long as k_{31}/k_{13} is constant). i_{+sat} increases as a function of $([S]_o k^o_{34} + k_{43})/k_{31}$ in the denominator, and Δi_{+sat} decreases as a function of $k_{31}/[S]_o k^o_{34}$ in the denominator. The ratios of k_{31} and $[S]_o k^o_{34}$ have the effect of scaling the positive saturation currents in relation to the corresponding negative currents. This leads to the conclusion that for small values of k_{31} operation of the reaction cycle in the reverse direction (clockwise) is also affected by solute changes outside. In other

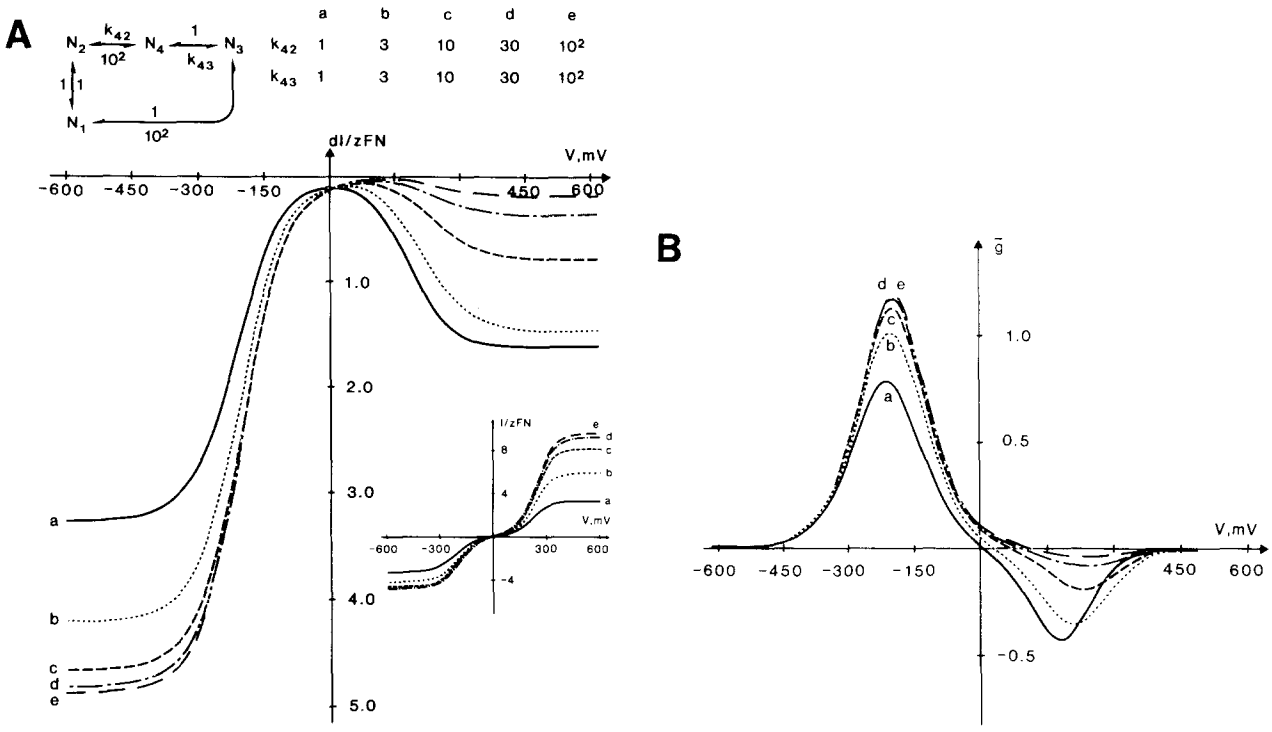

Fig. 6. *I-V* and *dI-V* dependence on proximity of the loaded carrier to the membrane charge-transit step. k_{42} and k_{43} increased in parallel over 2 orders of magnitude. (*A*) *dI-V* curves with parameter values as shown in the inset, upper left. Inset, lower right: corresponding 'plus solute' *I-V* curves. i_{+sat} and i_{-sat} increase in parallel as carrier state N_4 is functionally removed from the transport loop, but Δi_{+sat} and Δi_{-sat} are affected inversely. (*B*) $\bar{g}$-*V* profiles (arbitrary units) for *dI-V* curves in (*A*). Note the 120 mV-positive shift in the *apparent* E_c and small increase in the *dI-V* voltage-sensitive span ($\bar{s}$ = 405 mV (*a*), 450 mV (*e*))

words, the kinetic effect of solute addition is distributed between changes in carrier cycling in both directions.

From Fig. 5*A* and 5*B* it can be seen that changes in *dI-V* relations are restricted to Δi_{+sat}. Neither the $\bar{g}$ maximum or minimum displacements, nor the *V*-axis crossover point, are affected. In terms of the 2-state model, the effect of a hidden carrier state, occurring between carrier recycling and solute loading, appears in the empirical reaction constants κ_{io} and κ_{oi} only (compare with Fig. 3). It is of some interest, too, that the transporter in this case is likely to exhibit counterflow or exchange diffusion (*see* Sanders et al., 1984).

Proximity to Membrane Charge Transit of Solute Binding

Increasing the forward and reverse reaction constants k_{42} and k_{43} in concert when k_{24} is large results in parallel increases in both i_{+sat} and i_{-sat} in the *I-V* characteristics, but antiparallel changes in the corresponding currents for the *dI-V* curves (Fig. 6*A*). Formally, the effect on the difference current at large negative potentials results from the occurrence of k_{42} in both numerator and denominator of Eq. (24), which leads to an upper limit on Δi_{-sat} of $-zFN/2$. Equation (23), however, contains k_{43} in the numerator and k_{43}^2 in the denominator, and thus goes to zero as the reaction constant becomes large.

Intuitively, it can be seen that increases in k_{42} and k_{43} shift the steady-state distribution of carrier out of state N_4 and into state N_3, thus effectively eliminating the former from the loading/unloading arm of the cycle. Under these conditions, changes in the product $[S]_o k_{34}^o$ affect N_2 directly, leading to so-called "transfer" effects (Hansen et al., 1981): changes in carrier reloading appear displaced onto the charge-dependent limb of the reaction cycle. These circumstances will give rise to apparent kinetic equivalence of chemical and electrical driving forces (Hansen et al., 1981), observed both in primary and secondary transport processes (*cf.* Komor et al., 1979; Komor & Tanner, 1980; Maloney & Schattschneider, 1980; Maloney, 1982).

Of particular interest is the effect the reaction

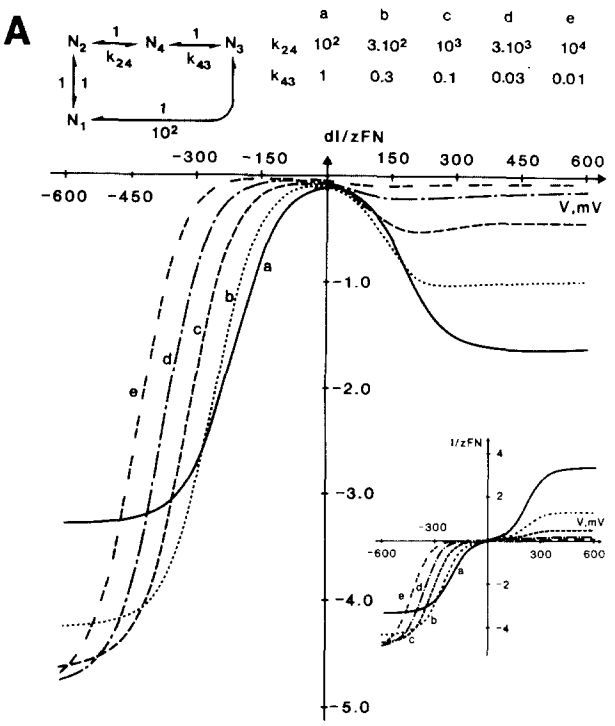

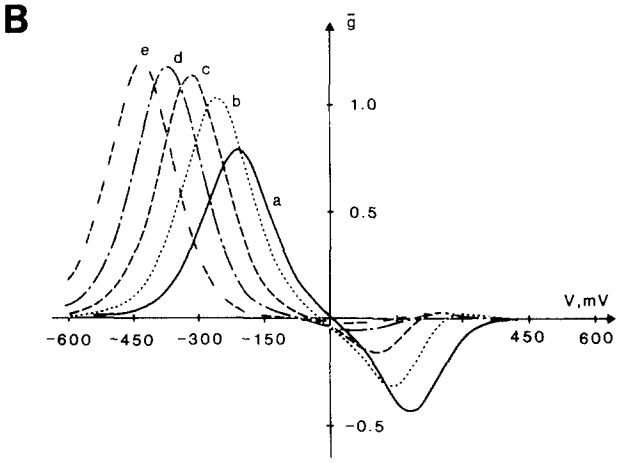

Fig. 7. *I-V* and *dI-V* dependence on loading of the solute-bound carrier state N_4. k_{24} increased and k_{43} decreased over 2 orders of magnitude. (*A*) *dI-V* curves with parameter values as shown in the upper left. Inset, lower right: corresponding 'plus solute' *I-V* curves. Current magnitudes at saturating voltages are affected similarly in the *I-V* and *dI-V* relations. *I-V* curve (*e*) indicates that the porter is largely irreversible. (*B*) $\bar{g}$-*V* profiles (arbitrary units) for the *dI-V* curves in *A*. The predominant effects of loading carrier state N_4 are a shift in the apparent E_c (−120 mV (*a* to *e*)) and an increase in the *dI-V* voltage-sensitive span ($\bar{s}$ = 405 mV (*a*), 488 mV (*e*)). (*C*) *dI-V* curves (*c*, *d* and *e*) plotted on expanded axes. The corresponding 'plus solute' *I-V* curve (dotted line) is included for *e* and shows the large voltage range near E_{trans} over which the difference curve departs from the *I-V* relation

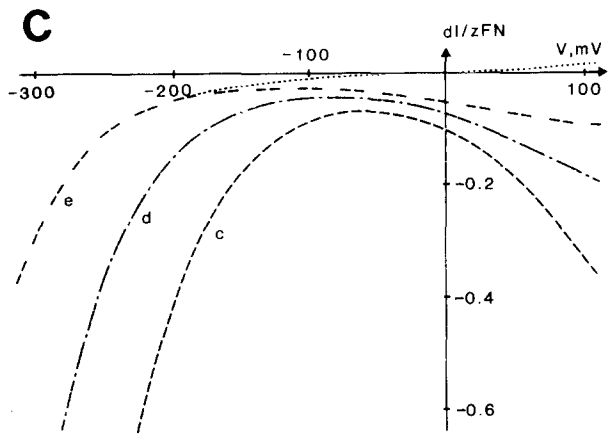

constants have on the *V*-axis crossover in the $\bar{g}$-*V* relations shown in Fig. 6*B*. Remember that for small values of k^o_{io} and k^o_{oi} this point is defined by E_c (=0 mV in the example). Increasing k_{42} and k_{43} over 2 orders of magnitude shifts the inflection point by +120 mV. Simultaneously, Δi_{-sat} and the $\bar{g}$ maximum rise, while Δi_{+sat} and the $\bar{g}$ minimum decrease in magnitude. In other words, roughly half the change associated with the sum of the constants k_{42} and k_{43} is displaced onto the charge-sensitive limb of the reaction cycle and leads to an *apparent* 100-fold increase in the ratio of empirical reaction constants k^o_{oi}/k^o_{io}.

Debinding-Rate-Limited Reverse Cycling

Figure 7 shows the effect of modifying the exterior debinding step k_{43} inversely with the reverse recycling step k_{24} on the current and conductance profiles. Increasing k_{24} and decreasing k_{43} when k_{31} and k_{42} are small has the predominant effect of increasing i_{-sat}, Δi_{-sat}, and the overall spread of the voltage-dependent regions in the *I-V* and *dI-V* characteristics, while reducing i_{+sat} and Δi_{+sat}. The effects on the currents at saturating membrane potentials result from the presence of the products $[S]_o k^o_{34} k_{24}$ in the denominator of i_{+sat} and $k_{43} k_{13}$ in the denomi-

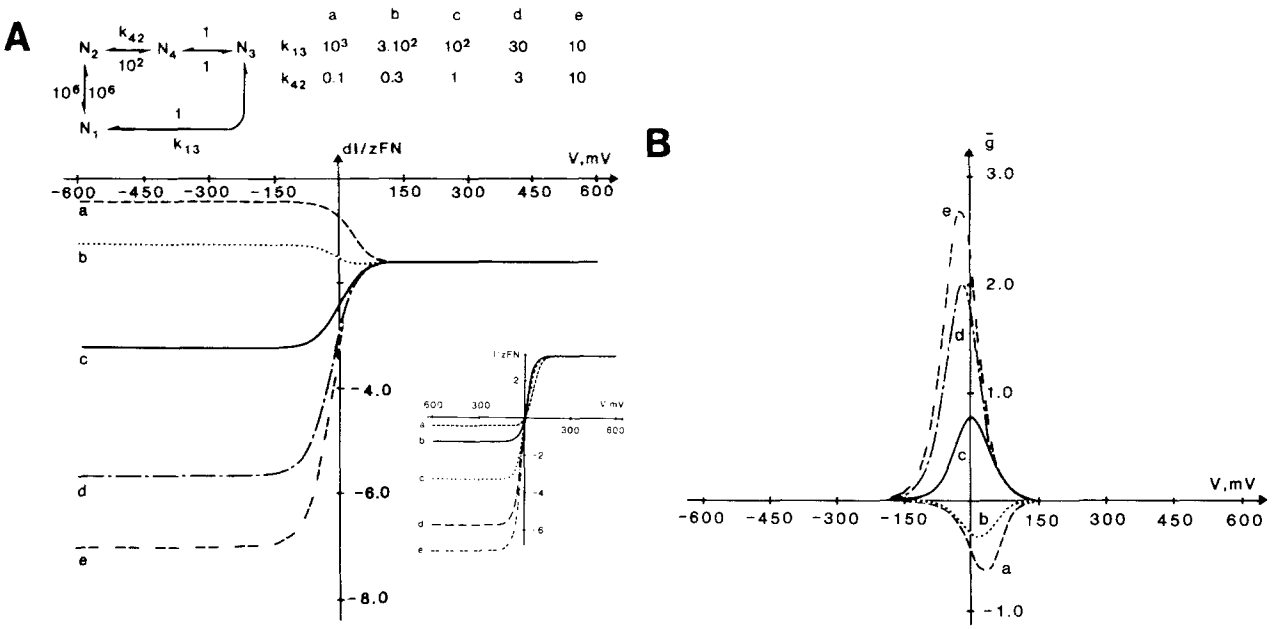

Fig. 8. *I-V* and *dI-V* dependence on hidden carrier states when membrane charge transit is inherently fast. k_{13} varied inversely with k_{42} over 2 orders of magnitude. (*A*) *dI-V* curves with parameter values shown in the upper left. Inset, lower right: corresponding 'plus solute' *I-V* curves. The primary effect, both in the *I-V* and *dI-V* relations, of loading carrier states N_3 and N_4 is on the currents at saturating negative voltages. Arrangements of reaction constants which strongly favor state N_4 yield *dI-V* profiles with a negative slope conductance only (curves *a* and *b*). (*B*) $\bar{g}$-*V* relations (arbitrary units) for the *dI-V* curves in (*A*). The apparent E_c shifts by *ca.* 30 mV for each 10-fold change in k_{13}

nator of $i_{-\text{sat}}$ (Eqs. 21, 22), and of the terms $[S]_o k_{34}^o$ and k_{43} in the denominator ratios for both $\Delta i_{-\text{sat}}$ and $\Delta i_{+\text{sat}}$ (Eqs. 23, 24).

More interesting is the increased voltage spread of the *I-V* and *dI-V* (*see* Fig. 7*A,B*) relations which can be understood in terms of an overall increase in the corresponding sum of empirical constants $\kappa_{io} + \kappa_{oi}$ relative to the charge-dependent steps (*see* Hansen et al., 1981, Table 1). Also apparent are decreases in the ratio k_{oi}^o/k_{io}^o between 1 and 0.01 as evidenced by shifts in the inflection points for the $\bar{g}$-*V* curves in Fig. 7*B*. There is nothing unusual in this situation. With $k_{24} \gg [S]_o k_{34}^o$, $k_{42} \gg k_{43}$ the carrier merely shows a pronounced tendency to reside on the outside of the membrane in the absence of a transmembrane electrical gradient. The modifications imposed may be seen, in contrast to the previous examples, to raise the solute binding constant (for a given $[S]_o$) at the expense of reverse cycle operation. Increasing k_{24}, in turn, affects the empirical ratios k_{oi}^o/k_{io}^o and $(\kappa_{io} + \kappa_{oi})/(k_{io}^o k_{oi}^o)^{1/2}$.

Qualitatively similar voltage spans are achieved by shifting the carrier bulk between N_3 and N_4 with appropriate weightings of k_{31}, k_{24} and k_{43} (or k_{34}^o); only the midpoint, defining the empirical ratio k_{oi}^o/k_{io}^o, is shifted along the voltage axis. Hence, it is clear that taken segmentally (even over a broad voltage span, say 250 mV, typical of studies in plant cells and fungi) current subtractions in any of these instances could mislead the experimenter to conclude that the porter operates as a current source far from equilibrium when the E_{trans} is in fact very near (*see* Fig. 7*C*). Misconceptions of this sort can lead to seemingly paradoxical situations when flux and electrical data are compared, and I return to this point in the Discussion.

Rapid Membrane Charge Transit and the Consequence of Hidden Carrier States

The circumstances described above are not the only ones yielding *dI-V* characteristics which parallel the voltage axis near E_{trans}. Arrangements of reaction constants which favor carrier states N_3 and N_4 will show apparent negative (inward) currents at all membrane potentials when k_{12}^o and k_{21}^o are large as well. The *I-V* and *dI-V* curves in Fig. 8 were obtained by setting these reaction constants to 10^6 and shifting the carrier bulk 'plus solute' between states $N_1 + N_2$ and $N_3 + N_4$ by modifying the forward reaction constants k_{13} and k_{42} inversely. This manipulation has the effect of scaling *the dI-V relations* according to $\Delta i_{+\text{sat}}$ while maintaining E_{trans} constant.

The *dI-V* curves show that solute 'addition' affects operation of the transporter proportionately less in the forward direction as carrier is shifted into N_4 in the steady state. Analogous variations in the currents at saturating membrane potentials are observed when k^o_{12} and k^o_{21} are small (*compare* conditions for the solid curves in Figs. 5*A*–7*A* with 8*A*); but now the *dI-V* relations are capable of showing little or no voltage-dependence *at any membrane potential* when the solute-loaded carrier state on the membrane exterior is heavily weighted.

Discussion

Voltage Sensitivity and E_{trans}

The most important conclusion to be drawn from the analytical treatment and examples above is that subtraction of steady-state *I-V* relations obtained through common experimental manipulations cannot yield meaningful transport reversal potentials directly. Specifically, this conclusion applies to conditions in which transport is modified asymmetrically with respect to reversible operation of the porter. Subtractions can give sensible reversal potentials—and *dI-V* characteristics which cross the voltage axis—when treatments inactivate or functionally remove transporter form the membrane. [Amiloride inhibition has been used in this fashion in studies of frog skin (Fuchs et al., 1977; Goudeau et al., 1982) to extract transcellular Na^+ currents. Likewise, ouabain binding to the animal Na^+,K^+-ATPase, which affects charge movements in both directions (Skou & Norby, 1979; Karlish & Stein, 1982), meets this criterion.] Kinetically, porter inactivation appears as a change in the scalar N and does not affect E_{trans}. Hence, the second assumption of proportionally altered currents outlined in the Introduction is met.

Difference-current-voltage relations cannot be expected to cross the voltage axis, however, when experimental modifications affect the net electrochemical driving force for transport. Such modifications include changes in transported solute (or driver ion) concentrations on one side of the membrane or, in the case of primary electrogenic ATPases, cytoplasmic ATP/ADP ratios. To date, an unambiguous demonstration of this point appears in a single study of potassium-proton cotransport in *Neurospora* (Blatt et al., 1984; Blatt & Slayman, 1986, and manuscript in preparation). In this case, potassium difference relations constructed from *I-V* curves gathered in the absence and presence of micromolar K^+ not only failed to cross the voltage axis at the predicted E_{K-H} (near −50 mV), but showed large and increasingly negative (inward) currents at more positive potentials. These *dI-V* profiles are unmistakably of the type shown in Figs. 3 and 5. Additionally, Hansen and Slayman (1978) have noted that *dI-V* curves for H^+-glucose cotransport in *Neurospora* failed to extrapolate to sensible reversal potentials and, analogous to the fungal K^+-H^+ porter, Beilby (1984, and *personal communications*) has observed that *dI-V* characteristics for the *Chara* proton pump consistently show increasingly positive (outward) currents at membrane potentials negative of −300 to −350 mV.

Apart from these observations, *dI-V* relations both for primary and secondary transport systems have generally revealed nothing unusual, presumably because the reversal potentials *expected* in most instances were situated well negative (Gradmann et al., 1978; Hansen et al., 1981) or positive (Walker et al., 1979; Felle, 1980, 1981*a*, 1982; Beilby & Walker, 1981; Sanders et al., Johannes & Felle, 1985) of the voltage ranges accessible to electrophysiological examination. Frequently, some degree of voltage dependence has been deduced from the difference currents, and extrapolating such curves to the voltage axis has often enough revealed 'reasonable' reversal potentials. In retrospect, however, such estimates must be treated with caution; reversal potentials obtained by this means are likely to be in error by tens, or perhaps hundreds of millivolts, even when voltage spans include a region of true voltage insensitivity. As a corollary to this point, it must be concluded, too, that *dI-V* relations which clearly *cross* the voltage axis (Roy & Okada, 1978; Beilby, 1984; Kishimoto et al., 1984; Takeuchi et al., 1985) include spurious currents from other membrane processes also affected by the experimental treatment.

Equally uninformative are situations in which the transporter appears to behave as a current source across the available voltage spectrum (Hansen & Slayman, 1978; Felle, 1981*a*,*b*, 1982; Sanders et al., 1983; Johannes & Felle, 1985). Difference current relations are readily derived which roughly parallel the voltage axis, over spans of 200 mV or more, *precisely in the region of the true* E_{trans} (*cf.* Figs. 3, 4 and 7). (Much broader regions of *apparent* voltage insensitivity are possible, too, if some degree of asymmetry is introduced into the Eyring barrier, so that e.g. $k_{12} = k^o_{12} \exp(\delta zu)$ and $k_{21} = k^o_{21} \exp((\delta - 1)zu)$, where $0 \leq \delta \leq 1$.) Furthermore, as rearrangements of Eqs. (13), (23) and (24) show, difference currents exhibit simple Michaelian kinetics with solute concentration at all membrane potentials. Thus, without complementary data from flux and biochemical (Hansen & Slayman, 1978) or

ion-sensitive electrode (Blatt et al., 1984; Rodriguez-Navarro et al., 1986) measurements, such featureless *dI-V* relations cannot be taken to indicate that the porter operates far from equilibrium.

Charge Stoichiometries and Chemical Fluxes

Difference current relations can also give rise to charge stoichiometries which vary with membrane potential, or to flux and electrical measurements which do not agree at all. A case in point is the H^+-glucose transporter of *Neurospora*. Hansen and Slayman (1978) observed that the influx of glucose dropped 20-fold under depolarizing conditions, despite the difference currents which, near 0 mV, indicated that sugar uptake should have been reduced by no more than 50% compared with measurements carried out in the normal potential range of −150 to −200 mV. A certain estimate of the E_{trans} was not possible in this instance (although it undoubtedly was situated positive of 0 mV), but similar studies with the nonmetabolizable analog 3-0-methyl glucose showed surprisingly little change in the *dI-V* relations as the solute accumulated in the cells.

Both sets of observations are most likely manifestations of the same problem: *near E_{trans} difference currents deviate from the true I-V characteristic for the porter*. Difference current relations for glucose transport (Figs. 2 and 3, Hansen & Slayman, 1978) are readily accommodated by curves of the sort shown in Fig. 7 above, which would account also for the paradoxical drop in flux measurements at low potentials compared with the difference currents. Likewise, *dI-V* relations are easily reconstructed for 3-0-methyl glucose transport to give comparably long regions of voltage sensitivity. The curves in Fig. 9 have been scaled to give currents at *ca.* −40 mV equivalent to those for 3-0-methyl glucose transport shortly after solute addition. E_{trans} values in the fitted *I-V curves* are comparable to those Hansen and Slayman estimated from tracer flux measurements. Extrapolating the fitted *dI-V curves* also *overestimates* E_{trans}, as was concluded for the experimental curves. [The small discrepancies apparent between modeled and experimental *dI-V* curves are consistent with the linearizing effect of point-clamping cylindrical cells (Smith, 1984).]

By the same token, charge stoichiometries determined near E_{trans} are likely to overestimate the true charge/chemical flux ratio. Subtracting currents over a broad voltage range may ensure, if the principle features of the *dI-V* characteristic can be determined, that the flux conditions chosen are sufficiently removed from equilibrium that *I-V* and *dI-V* characteristics coincide. The alternative of voltage clamping at a single potential throughout experimental manipulations (Jung et al., 1984) avoids this problem, but the resultant currents cannot be compared directly with chemical flux measurements obtained from nonvoltage-clamped cell suspensions. In practice, determining charge stoichiometries over a range of solute and/or driver ion concentrations provides a test against possible errors introduced by current subtractions (Rodriguez-Navarro et al., 1986).

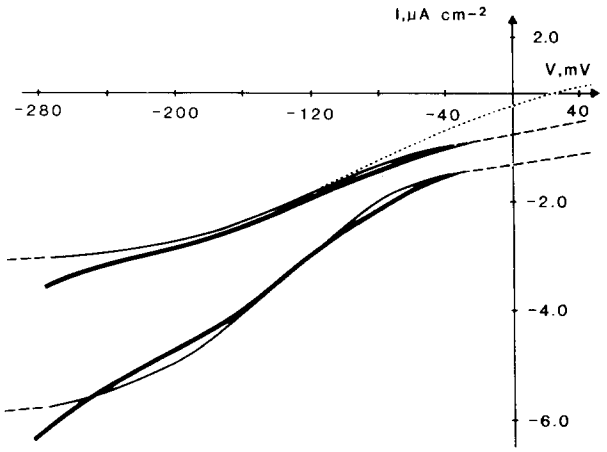

Fig. 9. Published and fitted *dI-V* curves for 3-0-methyl glucose transport in *Neurospora*. Heavy solid lines: data from Hansen and Slayman (1978, Fig. 5) redrawn for 0.5 and 2.5 mM 3-0-methyl glucose 30 sec after sugar additions. Light solid and dashed lines: fitted *dI-V* curves. Also shown is the 'plus solute' fitted *I-V* curve for the upper set of difference current relations. E_{trans} fitted and experimental (estimated), respectively: upper curves, +30 and +35 mV; lower curves, +69 and +76 mV. Values for the 4-state reaction constants 'minus solute': k^o_{12} = 0.3, k^o_{21} = 3, k_{13} = 200, k_{31} = 100, k_{24} = 50, k_{42} = 0.05, k_{34} = 0.0001, k_{43} = 0.002; k_{34} ('plus solute') increased to 0.03 for the upper *I-V* and *dI-V* curves, and to 0.15 for the lower *dI-V* curve before scaling to the experimental data (scale factor, $N = 10^{-8}$ mol m^{-2})

Extracting Empirical Constants from Experimental Data

Despite these cautionary notes, difference current relations can reveal considerable information about the kinetic properties of a transport system. The primary characteristics exhibited by *dI-V* curves have direct counterparts in their parent *I-V* curves in association with all four empirical reaction constants (Eqs. (12), (14)–(19), (25)–(28)). Two features only distinguish difference current relations. The first, relating to transport reversal potentials dis-

cussed above, implies that the products of forward and reverse reaction constants cannot be equated. The second is that subtraction alone cannot yield a value for the voltage-saturated current associated with reverse operation of the porter, κ_{oi} (or κ_{io} in the case of primary transport systems). To obtain κ_{io}, conditions can be chosen for which $\Delta i_{-\mathrm{sat}}$ closely approximates $i_{-\mathrm{sat}}$, but the remaining empirical constants are extractable in parameter ratios only. As a result, values for k_{io}^{o}, k_{oi}^{o}, κ_{oi} *and* E_{trans} must be resolved by statistically optimizing sets of *dI-V* curves obtained under well-defined conditions (*cf.* Gradmann et al., 1982).

Current subtractions, however, will implicate contributions from hidden carrier states, which become apparent in nonzero difference currents at saturating potentials for reverse cycle operation (Figs. 5–8 and accompanying discussions). This fact is particularly important since carrier distributions involving hidden states removed from the N_1-N_2 transition are likely to distort severely the apparent energy input associated with membrane charge transit. These circumstances are accommodated by "upgrading" the model to include additional carrier states, and by introducing new data such as might be obtained through variations in trans-ligand concentrations (*cf.* Requena, 1978; Komor et al., 1979; Sanders & Hansen, 1981; Beilby, 1984).

One important proviso applies to current substraction and its analysis. Current measurements must be carried out over a broad enough voltage span to reveal the dominant features in the *dI-V* relations. There is no hard and fast rule in this case, but some guidelines can be set based on the examples outlined above. Practically speaking, at least one region of voltage-saturated current and the E_c-associated conductance peak (or inflection point) are needed to establish the relations between reaction constants. Limiting spans for the voltage-dependent regions of the curves thus dictate a minimum sampling range near 300 mV if univalent transport processes are to be examined, but this value escalates rapidly when the possibility of slow membrane charge transit is taken into consideration.

Perhaps a better measure is gained from the studies already alluded to in this paper. Then sampling ranges of 300 mV, including the physiological voltage spectrum, are clearly too short and spans of 400 mV marginal only. Extending the voltage limits achieved experimentally is probably not a serious problem, however. Recent technical advances have enable routine examinations of *I-V* (and *dI-V*) proviles in *Chara* (Beilby, 1984) and *Neurospora* (Blatt et al., 1984; Blatt & Slayman, 1986) over membrane potentials between −400 and +100 mV. Equivalent voltage spans have also been attained in at least one higher plant cell type (Blatt, 1986), and there is good reason to believe future studies will meet with a similar degree of success.

I first realized the significance of subtracting currents in puzzling over *dI-V* curves for potassium transport in *Neurospora*. I am indebted to Dale Sanders (York) and Clifford Slayman (Yale) for introducing me to the kinetic model. My special thanks, also, to Mary Beilby for her enthusiasm, and to E.A.C. MacRobbie and to my wife for their patient support while I was preparing the manuscript.

References

Beilby, M. 1984. Current-voltage characteristics of the proton pump at *Chara* plasmalemma: I. pH Dependence. *J. Membrane Biol.* **81**:113–125

Beilby, M., Walker, N.A. 1981. Chloride transport in *Chara*. I: Kinetics and current-voltage curves for a probable proton symport. *J. Exp. Bot* **32**:43–54

Belkhode, M., Scholefield, P. 1969. Interactions between amino acids during transport and exchange diffusion in Novikoff and Ehrlich ascites tumor cells. *Biochim. Biophys. Acta* **173**:290–301

Bentrup, F.W. 1980. Electrogenic membrane transport in plants. A review. *Biophys. Struct. Mech.* **6**:175–189

Blatt, M. 1986. Calcium and the current-voltage relations of stomatal guard cells. *In:* Calcium in Plant Growth and Development. A. Trewavas, editor. Pergamon, Oxford (*in press*)

Blatt, M., Rodriguez-Navarro, A., Slayman, C.L. 1984. "Active" potassium uptake by *Neurospora* occurs in cotransport with protons. *Plant Physiol.* **75**:A902

Blatt, M., Slayman, C.L. 1986. Current-voltage analysis as a means to in vivo separation of primary and secondary coupled transport. *In:* Calcium in Plant Growth and Development. A. Trewavas, editor. Pergamon, Oxford (*in press*)

Chapman, J. 1982. A kinetic interpretation of "variable" stoichiometry for an electrogenic sodium pump obeying chemiosmotic principles. *J. Theor. Biol.* **95**:665–678

Chapman, J., Kootsey, J., Johnson, E. 1979. A kinetic model for determining the consequences of electrogenic active transport in cardiac muscle. *J. Theor. Biol.* **80**:405–424

Chapman, J.B., Johnson, E.A., Kootsey, J.M. 1983. Electrical and biochemical properties of an enzyme model of the sodium pump. *J. Membrane Biol.* **74**:139–154

Eddy, A. 1978. Proton-dependent solute transport in microorganisms. *Curr. Top. Membr. Transp.* **10**:279–360

Eddy, A. 1980. Slip and leak models of gradient-coupled transport. *Trans. Biochem. Soc. (London)* **8**:271–273

Epstein, E. 1976. Kinetics of ion transport and the carrier concept. *In:* Encyclopedia of Plant Physiology. M. Pitman and U. Lüttge, editors. Vol. 2B, pp. 70–94. Springer, Berlin

Felle, H. 1980. Amine transport at the plasmalemma of *Riccia fluitans*. *Biochim. Biophys. Acta* **602**:181–195

Felle, H. 1981*a*. Steriospecificity and electrogenicity of amino acid transport in *Riccia fluitans*. *Planta* **152**:505–512

Felle, H. 1981*b*. A study of the current-voltage relationships of electrogenic active and passive membrane elements in *Riccia fluitans*. *Biochim. Biophys. Acta* **646**:151–160

Felle, H. 1982. Effects of fusicoccin upon membrane potential,

resistance and current-voltage characteristics in root hairs of *Sinapis alba*. *Plant Sci. Lett.* **25**:219–225

Finkelstein, A. 1964. Carrier model for active transport of ions across a mosaic membrane. *Biophys. J.* **4**:421–440

Foster, D., Fillingame, R. 1979. Energy-transducing H^+-ATPase of *Escherichia coli*. *J. Biol. Chem.* **254**:8230–8236

Fuchs, W., Larsen, E.H., Lindemann, B. 1977. Current-voltage curve of sodium channels and concentration dependence of sodium permeability in frog skin. *J. Physiol. (London)* **267**:137–166

Giaquinta, R. 1980. Sucrose/proton cotransport during phloem loading and its possible control by internal sucrose concentration. *In:* Plant Membrane Transport: Current Conceptual Issues. R. Spanswick, W. Lucas, and J. Dainty, editors. pp. 273–282. Elsevier, Amsterdam

Goffeau, A., Slayman, C.W. 1981. The proton translocating ATPase of the fungal plasma membrane. *Biochim. Biophys. Acta* **639**:197–223

Goudeau, H., Wietzerbin, J., Mintz, E., Gingold, M.P., Nagel, W. 1982. Microelectrode studies of the effect of lanthanum on the electrical potential and resistance of outer and inner cell membranes of isolated frog skin. *J. Membrane Biol.* **66**:123–132

Gradmann, D. 1975. Analog circuit of the *Acetabularia* membrane. *J. Membrane Biol.* **25**:183–208

Gradmann, D., Hansen, U.-P., Long, W.S., Slayman, C.L., Warncke, J. 1978. Current-voltage relationships for the plasma membrane and its principal electrogenic pump in *Neurospora crassa*. I: Steady-state conditions. *J. Membrane Biol.* **39**:333–367

Gradmann, D., Hansen, U.-P., Slayman, C.L. 1982. Reaction kinetic analysis of current-voltage relationships for electrogenic pumps in *Neurospora* and *Acetabularia*. *Curr. Top. Membr. Transp.* **16**:257–281

Hajjar, J., Lamont, A., Curran, P. 1970. The sodium-alanine interaction in rabbit illium: Effect of sodium on alanine fluxes. *J. Gen. Physiol.* **55**:277–296

Hansen, U.-P., Gradmann, D., Sanders, D., Slayman, C.L. 1981. Interpretation of current-voltage relationships for "active" ion transport systems: I. Steady-state reaction-kinetic analysis of class-I mechanisms. *J. Membrane Biol.* **63**:165–190

Hansen, U.-P., Slayman, C.L. 1978. Current-voltage relationships for a clearly electrogenic cotransport system. *In:* Membrane Transport Processes. J.F. Hoffman, editor. Vol. 1, pp. 141–154. Raven, New York

Hill, T.L., Eisenberg, E. 1981. Can energy transduction be localized at some crucial part of the enzymatic cycle? *Q. Rev. Biophys.* **14**:463–511

Johannes, E., Felle, H. 1985. Transport of basic amino acids in *Riccia fluitans:* Evidence for a second binding site. *Planta* **166**:244–251

Jung, D., Schwarz, W., Passow, H. 1984. Sodium-alanine cotransport in oocytes of *Xenopus laevis:* Correlation of alanine and sodium fluxes with potential and current changes. *J. Membrane Biol.* **78**:29–34

Kaczorowski, G., Robertson, D., Garcia, M., Padan, E., Patel, L., Le Blanc, G., Kaback, H.R. 1980. Energetics and mechanism of lactose translocation in isolated membrane vesicles of *Escherichia coli*. *Ann. N.Y. Acad. Sci.* **358**:307–321

Karlish, S., Stein, W. 1982. Protein conformational changes in (Na,K)-ATPase and the role of cation occlusion in active transport. *Ann. N.Y. Acad. Sci.* **402**:226–238

Keifer, D., Spanswick, R. 1979. Correlation of adenosine triphosphate levels in *Chara corallina* with the activity of the electrogenic pump. *Plant Physiol.* **64**:165–168

Kinne, R. 1976. Properties of the glucose transport system in the renal brush border membrane. *Curr. Top. Membr. Transp.* **8**:209–267

Kishimoto, U., Kami-ike, N., Takeuchi, Y., Ohkawa, T. 1984. A kinetic analysis of the electrogenic pump of *Chara corallina:* I. Inhibition of the pump by DCCD. *J. Membrane Biol.* **80**:175–183

Komor, E., Schwab, W., Tanner, W. 1979. The effect of intracellular pH on the rate of hexose uptake in *Chlorella*. *Biochim. Biophys. Acta* **555**:524–530

Komor, E., Tanner, W. 1974. The hexose-proton cotransport system of *Chlorella*. pH-dependent change in K_m values and translocation constants of the uptake system. *J. Gen. Physiol.* **64**:568–581

Komor, E., Tanner, W. 1980. Proton-cotransport of sugars in plants. *In:* Plant Membrane Transport: Current Conceptual Issues. R. Spanswick, W. Lucas, and J. Dainty, editors. pp. 247–257. Elsevier, Amsterdam

Kostyuk, P., Krishtal, O., Pidoplichko, V. 1972. Potential-dependent membrane current during the active transport of ions in snail neurones, *J. Physiol. (London)* **226**:373–392

Lanyi, J. 1978. Coupling of aspartate and serine transport to the transmembrane electrochemical gradient for sodium ions in *Halobacterium halobium*. Translocation stoichiometries and apparent cooperativity. *Biochemistry* **17**:3011–3018

Lanyi, J., MacDonald, R. 1976. Existence of electrogenic hydrogen ion/sodium ion antiport in *Halobacterium halobium* cell envelope vesicles. *Biochemistry* **15**:4608–4613

Lass, B., Ullrich-Eberius, C. 1984. Evidence for proton/sulfate cotransport and its kinetics in *Lemna gibba* G1. *Planta* **161**:53–60

Läuger, P. 1979. A channel mechanism for electrogenic ion pumps. *Biochim. Biophys. Acta* **552**:143–161

Läuger, P. 1980. Kinetic properties of ion carriers and channels. *J. Membrane Biol.* **57**:163–178

Läuger, P., Stark, G. 1970. Kinetics of carrier-mediated ion transport across lipid bilayer membranes. *Biochim. Biophys. Acta* **211**:458–466

Le Blanc, G., Rimon, G., Kaback, H.R. 1980. Glucose 6-phosphate transport in membrane vesicles isolated from *Escherichia coli:* Effect of imposed electrical potential and pH gradient. *Biochemistry* **19**:2522–2528

Maloney, P. 1982. Energy coupling to ATP synthesis by the proton-translocating ATPase. *J. Membrane Biol.* **67**:1–12

Maloney, P., Schattschneider, S. 1980. Voltage sensitivity of the proton-translocating adenosine 5′-triphosphatase in *Streptococcus lacits*. *FEBS Lett.* **110**:337–340

Mandel, L., Curran, P. 1973. Response of the frog skin to steady-state voltage-clamping. II. The active pathway. *J. Gen. Physiol.* **62**:1–24

Marmor, M. 1971. The independence of electrogenic sodium transport and membrane potential in a molluscan neurone. *J. Physiol. (London)* **218**:599–608

Milanick, M., Gunn, R. 1982. Proton-sulfate co-transport. Mechanism of H^+ and sulfate addition to the chloride transporter of human red blood cells. *J. Gen. Physiol.* **79**:87–113

Mitchell, P. 1969. Chemiosmotic coupling and energy transduction. *Theor. Exp. Biophys.* **2**:159–216

Morrison, C., Lichstein, H. 1976. Regulation of lysine transport by feedback inhibition in *Saccharomyces cerevisiae*. *J. Bacteriol.* **125**:864–871

Page, M., West, I. 1981. The kinetics of the β-galactoside-proton symport of *Escherichia coli*. *Biochem. J.* **196:**721–731

Pall, M. 1971. Amino acid transport in *Neurospora crassa:* IV. Properties and regulation of a methionine transport system. *Biochim. Biophys. Acta* **233:**201–214

Reichert, U., Schmidt, R., Foret, M. 1975. A possible mechanism of energy coupling in purine transport of *Saccharomyces cerevisiae*. *FEBS Lett.* **52:**100–102

Reid, R., Walker, N.A. 1983. Adenylate concentrations in *Chara:* Variability, effects of inhibitors and relationship to protoplasmic streaming. *Aust. J. Plant Physiol.* **10:**373–383

Requena, J. 1978. Calcium efflux from squid axons under constant sodium electrochemical gradient. *J. Gen. Physiol.* **72:**443–470

Rodriguez-Navarro, A., Blatt, M., Slayman, C.L. 1986. A potassium-proton cotransporter in *Neurospora*. *J. Gen. Physiol.* (*in press*)

Rodriguez-Navarro, A., Ramos, J. 1984. Dual system for potassium transport in *Saccharomyces cerevisiae*. *J. Bacteriol.* **159:**940–945

Roy, G., Okada, Y. 1978. Oscillation of membrane potential in L cells: III. K^+ current-voltage curves. *J. Membrane Biol.* **38:**347–357

Sanders, D. 1980*a*. Control of Cl^- influx in *Chara* by cytoplasmic Cl^- concentration. *J. Membrane Biol.* **52:**51–60

Sanders, D. 1980*b*. The mechanism of Cl^- transport at the plasma membrane of *Chara corallina:* I. Cotransport with H^+. *J. Membrane Biol.* **53:**129–141

Sanders, D., Hansen, U.-P. 1981. Mechamism of Cl transport at the plasma membrane of *Chara corallina:* II. Transinhibition and the determination of H^+/Cl^- binding order from a reaction kinetic model. *J. Membrane Biol.* **58:**139–153

Sanders, D., Hansen, U.P., Gradmann, D., Slayman, C.L. 1984. Generalized kinetic analysis of ion-driven cotransport systems: A unified interpretation of selective ionic effects on Michaelis parameters. *J. Membrane Biol.* **77:**123–152

Sanders, D., Slayman, C.L., Pall, M. 1983. Stoichiometry of H^+/amino acid cotransport in *Neurospora crassa* revealed by current-voltage analysis. *Biochim. Biophys. Acta* **735:**67–76

Skou, J., Norby, J. 1979. Na/K-ATPase: Structure and Kinetics. Academic, New York

Smith, J.R. 1984. The electrical properties of plant cell membranes. II. Distortion of non-linear current-voltage characteristics induced by the cable properties of *Chara*. *Aust. J. Plant Physiol.* **11:**211–224

Takeuchi, Y., Kishimoto, U., Ohkawa, T., Kami-ike, N. 1985. A kinetic analysis of the electrogenic pump of *Chara corallina:* II. Dependence of the pump activity on external pH. *J. Membrane Biol.* **86:**17–26

Ullrich-Eberius, C., Novacky, A., van Bel, A. 1984. Phosphate uptake in *Lemna gibba* G1: Energetics and kinetics. *Planta* **161:**46–52

Walker, N.A., Beilby, M.J., Smith, F.A. 1979. Amine uniport at the plasmalemma of Charophyte cells: I. Current-voltage curves, saturation kinetics, and effects of unstirred layers. *J. Membrane Biol.* **49:**21–55

West, I. 1980. Energy coupling in secondary active transport *Biochim. Biophys. Acta* **604:**91–126

Received 6 December 1985; revised 13 March 1986